



## Review

Structure and function of preQ<sub>1</sub> riboswitches<sup>☆</sup>Catherine D. Eichhorn<sup>a,1</sup>, Mijeong Kang<sup>a,b,1</sup>, Juli Feigon<sup>a,b,\*</sup><sup>a</sup> Department of Chemistry and Biochemistry, University of California, Los Angeles, CA 90095, USA<sup>b</sup> UCLA-DOE Institute for Genomics and Proteomics, University of California, Los Angeles, CA 90095, USA

## ARTICLE INFO

## Article history:

Received 6 February 2014

Received in revised form 22 April 2014

Accepted 25 April 2014

Available online 4 May 2014

## Keywords:

Queuosine

tRNA modification

NMR

X-ray crystallography

Queuine

PreQ<sub>0</sub>

## ABSTRACT

PreQ<sub>1</sub> riboswitches help regulate the biosynthesis and transport of preQ<sub>1</sub> (7-aminomethyl-7-deazaguanine), a precursor of the hypermodified guanine nucleotide queuosine (Q), in a number of Firmicutes, Proteobacteria, and Fusobacteria. Queuosine is almost universally found at the wobble position of the anticodon in asparaginyl, tyrosyl, histidyl and aspartyl tRNAs, where it contributes to translational fidelity. Two classes of preQ<sub>1</sub> riboswitches have been identified (preQ<sub>1</sub>-I and preQ<sub>1</sub>-II), and structures of examples from both classes have been determined. Both classes form H-type pseudoknots upon preQ<sub>1</sub> binding, each of which has distinct unusual features and modes of preQ<sub>1</sub> recognition. These features include an unusually long loop 2 in preQ<sub>1</sub>-I pseudoknots and an embedded hairpin in loop 3 in preQ<sub>1</sub>-II pseudoknots. PreQ<sub>1</sub>-I riboswitches are also notable for their unusually small aptamer domain, which has been extensively investigated by NMR, X-ray crystallography, FRET, and other biophysical methods. Here we review the discovery, structural biology, ligand specificity, cation interactions, folding, dynamics, and applications to biotechnology of preQ<sub>1</sub> riboswitches. This article is part of a Special Issue entitled: Riboswitches.

© 2014 Elsevier B.V. All rights reserved.

## 1. Introduction

The prequeuosine 1 (preQ<sub>1</sub>) riboswitch is a member of a large sub-set of riboswitches that are involved in the regulation of purine synthesis and transport [1,2]. These include riboswitches whose aptamer domain recognizes the base adenine or guanine, the nucleoside 2'-deoxyguanosine, the second messenger cyclic-di-GMP, and the modified guanine preQ<sub>1</sub>, as well as the purine moiety of the co-factors S-adenosylmethionine, S-adenosylhomocysteine, and adenosylcobalamin [1,2]. PreQ<sub>1</sub> riboswitches help regulate the biosynthesis and transport of preQ<sub>1</sub> (7-aminomethyl-7-deazaguanine), a precursor of the hypermodified guanine nucleotide queuosine (Q). Q is almost universally found in prokaryotes and eukaryotes (but not archaea, which utilize the Q homolog archaeosine [3]) in asparaginyl, tyrosyl, histidyl and aspartyl tRNAs at the anticodon wobble position [4–7] (Fig. 1A).

Modified nucleotides are found in all classes of RNA molecules and are essential for normal cellular function [8]. tRNAs are the most highly modified RNAs, containing on average 13 modified nucleotides per tRNA from over 100 unique RNA modifications [9]. These modifications contribute to tRNA stability [10], prevent ribosomal frameshifting [11], increase translation efficiency and fidelity [12], and improve anticodon–codon recognition [13]. Nearly all tRNAs contain a modification

at the wobble position of the anticodon [14]. These modifications, including Q, are believed to influence the stability of the anticodon–codon interaction and promote translation accuracy. Q has been implicated to play a role in eukaryotic cellular development and proliferation [15–21], relieving hypoxic stress [22], neoplastic transformation [18, 23–27], tyrosine biosynthesis [28], translation frameshifting required in retroviral protein synthesis [29], and virulence of pathogenic bacteria such as *Shigella flexneri* [30–33] (reviewed in [8,34]).

Prokaryotes synthesize preQ<sub>1</sub> de novo from GTP in a multienzyme pathway (Fig. 1B) (reviewed in [35]). First, preQ<sub>0</sub> is synthesized in a series of reactions successively involving GTP cyclohydrolase (GCH1), 6-carboxy-5,6,7,8-tetrahydropterin synthase (QueD), 7-carboxy-7-deazaguanine (CDG) synthase (QueE), and preQ<sub>0</sub> synthase (QueC), which replaces the guanine N7 with an acetonitrile group, in a pathway that was recently elucidated [35]. PreQ<sub>0</sub> is converted to preQ<sub>1</sub> by the preQ<sub>0</sub> reductase (QueF), which reduces the nitrile group to an exocyclic aminomethyl substituent. The free base preQ<sub>1</sub> is then directly attached to the wobble position of the anticodon of cognate tRNAs by tRNA:guanine transglycosylase (TGT), which catalyzes the posttranscriptional exchange of guanine with preQ<sub>1</sub>. The exocyclic amine at the 7 position is then modified by S-adenosylmethionine:tRNA ribosyltransferase-isomerase (QueA) to epoxyqueuosine-tRNA, and finally epoxyqueuosine (oQ) is converted to Q by oQ reductase (QueG). The cyclopentadiol substituent of Q is sometimes further modified in certain organisms with a glutamate, mannose, or galactosyl group [36,37]. Because eukaryotes do not synthesize queuosine precursors de novo but rather scavenge Q from their diet or intestinal flora as the free base, queuine, preQ<sub>1</sub> riboswitches are only found in prokaryotes.

<sup>☆</sup> This article is part of a Special Issue entitled: Riboswitches.

\* Corresponding author at: Department of Chemistry and Biochemistry, University of California, Los Angeles, CA 90095, USA.

<sup>1</sup> Equal contribution.

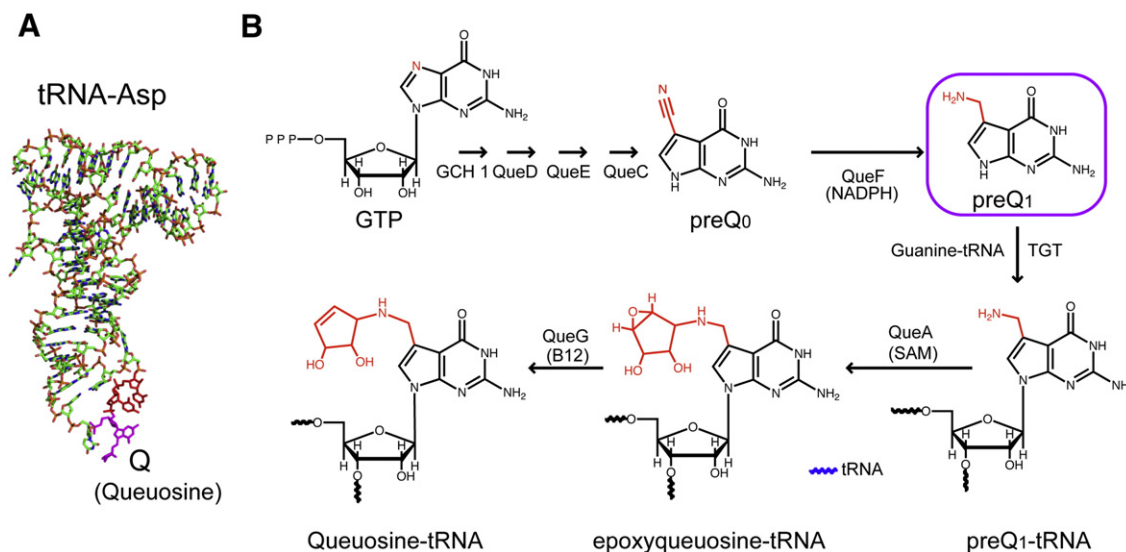


**Fig. 1.** Structure and synthesis of queuosine in bacteria. (A) Structure of aspartyl tRNA with queuosine at the wobble position of the anticodon highlighted in magenta. (B) Pathway for synthesis of queuosine, highlighting the structures of preQ<sub>0</sub> and preQ<sub>1</sub>.

Two classes of preQ<sub>1</sub> riboswitches have been identified (preQ<sub>1</sub>-I and preQ<sub>1</sub>-II) with distinct aptamer secondary and tertiary structures. The preQ<sub>1</sub>-I riboswitches have the smallest known aptamer domain discovered to date, which has facilitated numerous biophysical and computational modeling studies on structure and folding. The larger preQ<sub>1</sub>-II riboswitch aptamer provides an interesting example of convergent evolution, utilizing a distinct mode of ligand recognition from the preQ<sub>1</sub>-I riboswitch. Here we review X-ray crystal and NMR solution structures of preQ<sub>1</sub>-I and preQ<sub>1</sub>-II riboswitches and what has been learned from structural and biophysical studies about preQ<sub>1</sub> riboswitch folding, dynamics, cation interactions, specificity of ligand binding, and potential applications to biotechnology.

## 2. Identification of preQ<sub>1</sub> riboswitches and sequence conservation

PreQ<sub>1</sub>-I riboswitches were first identified in a bioinformatics survey of noncoding DNA regions across 91 microbial genomes, and were commonly found in the 5' UTR of the *ykjJKLM* operon encoding QueC, QueD, QueE, and QueF [38,39]. The unusually small size of the aptamer (later determined to be minimally 34 nucleotides (nt)) [39] posed a challenge in the initial survey, and the preQ<sub>1</sub>-I motif was only observed in a few species in the orders Bacillales and Clostridia; upon revision of the initial search algorithm preQ<sub>1</sub> riboswitches were identified across the phyla Firmicutes, Proteobacteria, and Fusobacteria [39]. PreQ<sub>1</sub>-I riboswitches were initially sorted into two types, types 1 and 2. These two types are highly similar and differ mainly in the conserved apical loop sequence [39]. However, the solved preQ<sub>1</sub>-bound structures of types 1 and 2 are nearly identical, and some riboswitches share type 1 and type 2 features. These types are combined in the Rfam database and fall under the generic preQ<sub>1</sub>-I class; to date, nearly 900 sequences across 647 species have been identified for preQ<sub>1</sub>-I riboswitches [40]. Phylogenetic analysis showed that the preQ<sub>1</sub>-I riboswitches have a conserved secondary structure of a hairpin (P1) followed by an A-rich sequence (Fig. 2A). The P1 hairpin is often preceded by a P0 hairpin (Fig. 2C), which is not required for ligand binding and has only a small effect on K<sub>d</sub> (~2-fold) [39].

A second class of preQ<sub>1</sub> riboswitches (preQ<sub>1</sub>-II) with a different conserved sequence, secondary structure, and apparently different mode of recognition was found associated with the COG4708 gene family, which is a family of membrane proteins predicted to be involved in Q transport [41,42]. This motif appears to be much more limited across phylogeny and has only been identified in the families Streptococcaceae and Lactobacillaceae within the order Lactobacillales; to date, 429 sequences

across 423 species have been identified for preQ<sub>1</sub>-II riboswitches in the Rfam database [40]. PreQ<sub>1</sub>-II riboswitches have a conserved secondary structure of three hairpins (P1, P2, and P4) and a potential pseudoknot hairpin (P3) (Fig. 2B). Similar to the P0 hairpin in the preQ<sub>1</sub>-I riboswitch, the P1 stem is dispensable for preQ<sub>1</sub> binding in vitro [42–44]. While preQ<sub>1</sub>-I riboswitches have been identified that regulate transcription or translation (Fig. 2C, D), preQ<sub>1</sub>-II riboswitches identified to date are only involved in translation regulation (Fig. 2D).

## 3. The preQ<sub>1</sub>-I riboswitch

### 3.1. PreQ<sub>1</sub>-I aptamer structures

Structures of ligand-bound preQ<sub>1</sub>-I riboswitch aptamers were reported from three laboratories at about the same time: the X-ray crystal and NMR solution structures of a transcription-regulating *Bacillus subtilis* (*Bsu*) riboswitch (type 2) bound to preQ<sub>1</sub> [45,46] and the X-ray crystal structure of a translation-regulating *Thermoanaerobacter tengcongensis* (*Tte*) riboswitch (type 1) bound to preQ<sub>0</sub> [47] (Table 1). A crystal structure of the *Tte* riboswitch bound to preQ<sub>1</sub> was later reported [48], and below we first compare the preQ<sub>1</sub>-bound riboswitch structures (Fig. 3). All of these structures were determined from minimal aptamer sequences, identified by in-line probing and deletions of the *Bsu* riboswitch [39], which did not include the putative P0 helix. The structures revealed that in the presence of preQ<sub>1</sub> the 3' end of the A-rich tail of the preQ<sub>1</sub>-I aptamer base pairs with the center of the P1 hairpin loop to form an H-type pseudoknot with two stems (stem 1 and stem 2) and three loops (loop 1, 2, and 3), and together provided detailed insight into the determinants of ligand recognition (Fig. 3). Evidence for pseudoknot formation in the presence of preQ<sub>1</sub> was also shown for a *Fusobacterium nucleatum* (*Fnu*) preQ<sub>1</sub>-I riboswitch (type 2) by imino proton NMR studies of site-specifically <sup>15</sup>N-labeled RNA [49].

Two crystal structures of the *Bsu* riboswitch aptamer were determined, one of the wild-type (WT) sequence (*Bsu* WT) (Fig. 3C–D) and the other of a loop 2 sequence variant (*Bsu* L2var), where the central four of the six loop 2 nts are substituted, which diffracted to higher resolution (Table 1). The NMR structure has two nt substitutions in loop 2, C12U and C15U (*Bsu* C12,15U), and has two additional Gs at the 5' end that precede the P1 stem in the WT sequence (Fig. 3A–B). Only the last residue of loop 2 (C17) is highly conserved and these differences have little effect on the structures, but they do impact folding and apparent ligand affinity, as discussed in Section 3.5. The crystal and solution structures of the *Bsu* riboswitch are nearly identical (Fig. 3A–D), with small

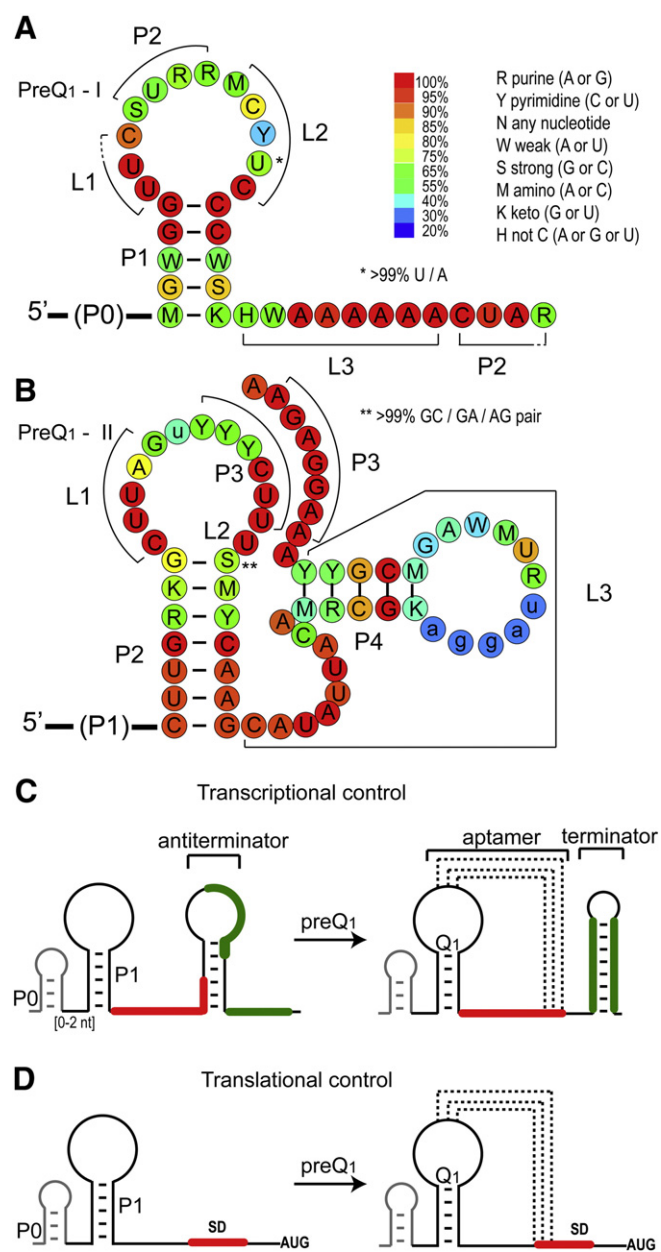


**Fig. 2.** Predicted secondary structure, sequence conservation, and gene regulatory mechanism of preQ<sub>1</sub> riboswitches. (A,B) Sequence conservation of riboswitch aptamer domains of preQ<sub>1</sub>-I (A) and preQ<sub>1</sub>-II (B). Sequence conservation is from 894 sequences from 647 species for preQ<sub>1</sub>-I and 429 sequences from 423 species for preQ<sub>1</sub>-II from the Rfam database (1/31/2014) <http://rfam.sanger.ac.uk/>. (C,D) Schematic of gene regulation by preQ<sub>1</sub>-I riboswitches for (C) transcription or (D) translation. The antiterminator in (C) and mechanism for regulation were revealed from structural studies [45,46].

but significant differences in the positions of residues in the upper part of the pseudoknot, discussed below. The structure of the Tte riboswitch (Tte WT) is also highly similar to the Bsu riboswitch structures with a nearly identical binding pocket despite sequence differences, particularly in the residues above the binding pocket (Fig. 3E, F).

In the solved pseudoknot structures, stem 1 is 5 bp, stem 2 is 3–4 bp, loop 1 is 2–3 nt, loop 2 is 4–6 nt, and loop 3 is 8–9 nt. Stems 1 and 2 form a continuous stack with preQ<sub>1</sub> inserted at the junction between them, where it forms a Watson–Crick (WC) base pair (bp) with the last base of loop 2 (C17 in Bsu, C15 in Tte) (Fig. 3A, C, E). As is usual for H-type pseudoknots loop 1 lies along the major groove and loop 3 lies along the minor groove, and loop 3 has extensive interactions with the bases in stem 1 (Fig. 3A–F). Loop 2 connects stem 1 and stem 2, and is

absent or short (0–2 nt) in most H-type pseudoknots. The unusually long loop 2 in the preQ<sub>1</sub>-I riboswitch aptamer, which is largely looped out near the minor groove, likely explains why this pseudoknot fold was not predicted and is important for how the riboswitch functions in gene regulation, as discussed in Section 3.5. Another important feature is the short stem 2, which in the Bsu riboswitch has only 3 WC bp and two non-WC bps (Fig. 3A–F). Thus, stem 2 would be intrinsically unstable in the absence of tertiary interactions from loops 1 and 2.

The first 8–9 residues of the A-rich tail that follows the P1 hairpin form loop 3, while the 3' end of the tail pairs with the center of the P1 hairpin loop to form P2, with the residues on the 5' and 3' sides of that hairpin loop comprising loop 1 and loop 2, respectively (Fig. 2A). Loop 3 is highly conserved and A-rich (7 of 8 nts in Bsu, 6 of 9 nts in Tte) and interacts along the length of the minor groove of the 5 bp stem 1, notably through many adenine NH<sub>2</sub> interactions with the sugar edge (N3 of A, O2 of C or U, 2'OH) of bases in stem 1 (A amino-kissing motif) (Fig. 3A, C, E, I). Loop 2 is 6 nts in the Bsu riboswitch and 4 nts in the Tte riboswitch. The only highly conserved residue in this loop, the last residue C17 (C15 in Tte), forms a WC bp with preQ<sub>1</sub>. The two adenine residues in loop 2 interact in the minor groove of stem 2, forming a continuous stack with C17: A14 (A13 in Tte) has an A-minor interaction with U32 2'OH (U31 in Tte); A16 (A14 in Tte) forms an A–G–C triple, *trans* WC-sugar edge (Fig. 3G). In the solution structure of Bsu (C12,15U) the bases of the remaining three loop 2 nts (12, 13, 15) are flipped out. In the crystal structure of Bsu WT, C12, U13, and the base of C15 are crystallographically disordered while for Bsu L2var all of loop 2 are crystallographically disordered except for C17. Thus, loop 2 is partially dynamic, as discussed in Section 3.5. The shorter Tte loop lacks two of the pyrimidine residues but has a similar 3 nt stack with the remaining nt (U12) flipped out [47].

Loop 1 is short (2–3 residues), runs from the top of P1 to the top of P2, and forms a tight turn in the major groove of P2. The first residue, U6, interacts with preQ<sub>1</sub> and loop 3 residue A29 (A28 in Tte). In the crystal structures of the Bsu riboswitches, U7 hydrogen bonds to the Hoogsteen edge of A30 (the last residue of loop 3) and C8 pairs with A34 at the top of P2. In the solution structure of the Bsu C12,15U riboswitch, the positions of U7 and C8 are dynamic, the backbone turn is less sharp, and C8 is not within base pairing distance of A34. An NMR study in which the Bsu solution and crystal structures were rigorously compared using experimental and calculated residual dipolar couplings (RDCs), which provide information on the orientation of each bond vector, confirmed that these differences are largely due to Ca<sup>2+</sup>-induced structural changes [50], as discussed in Sections 3.4 and 3.5. As this is the only example where the structure of the same riboswitch has been determined both by NMR and crystallography, it is worth noting that the RDC analysis also confirmed that the bottom half of the riboswitches, including P1 and loop 3, are virtually identical in solution and in the crystal. In the Tte riboswitch, the corresponding loop 1 residues C7 and G8 interact with the bottom half of stem 2 (Fig. 3E, F).

### 3.1.1. The preQ<sub>1</sub> binding pocket

The preQ<sub>1</sub> binding pocket can be described as three layers (Fig. 3G–I), the preQ<sub>1</sub> 'binding core' where preQ<sub>1</sub> hydrogen bonds to one residue from each of the three loops to form a preQ<sub>1</sub>-C–A–U base quartet (Fig. 3H), the 'floor' of the binding pocket where the C–G bp at the top of stem 1 forms an A–C–G–A base quartet with two successive As from loop 3 (Fig. 3I), and the 'ceiling' where the G–C bp at the bottom of stem 2 forms an A–G–C triple (A–G–C–C quartet in Tte) above the binding core (Fig. 3G). In the binding core, specificity for preQ<sub>1</sub> is achieved by hydrogen bonds to all of the proton donors and acceptors of the preQ<sub>1</sub> ring. The last C in loop 2 (C17 in Bsu, C15 in Tte) interacts via a standard WC bp, the last A in loop 3 (A30 in Bsu, A29 in Tte) and first U in loop 1 (U6) hydrogen bond to the sugar edge of preQ<sub>1</sub> (Fig. 3H). In the Bsu riboswitch structures, the exocyclic amine group of preQ<sub>1</sub> points out of

**Table 1**  
Structures of preQ<sub>1</sub> riboswitches.

Class	Organism	Method	PDB	Ions in structures (cations in buffer)	Ligand	Name (# nts)	Ref
I	<i>Bsu</i>	X-ray	3FU2	Ca <sup>2+</sup> (Mg <sup>2+</sup> )	PreQ <sub>1</sub>	Bsu WT (34)	[46]
I	<i>Bsu</i>	X-ray	3K1V	Ca <sup>2+</sup> (Mg <sup>2+</sup> )	PreQ <sub>1</sub>	Bsu L2var L2:A13C14A15U16 <sup>a</sup> (34)	[46]
I	<i>Bsu</i>	NMR	2L1V	(K <sup>+</sup> )	PreQ <sub>1</sub>	Bsu C12,15U (36, with 5' GG)	[45,50]
I	<i>Tte</i>	X-ray	3Q50	SO <sub>4</sub> <sup>2-</sup> (Mg <sup>2+</sup> )	PreQ <sub>1</sub>	Tte WT (33)	[48]
I	<i>Tte</i>	X-ray	3GCA	SO <sub>4</sub> <sup>2-</sup> (Mg <sup>2+</sup> )	PreQ <sub>0</sub>	Tte WT (33)	[47]
I	<i>Tte</i>	X-ray	3Q51	SO <sub>4</sub> <sup>2-</sup> , Mg <sup>2+</sup>	None	Tte WT (33)	[48]
II	<i>Lra</i>	X-ray	4JF2	Mg <sup>2+</sup> , Cs <sup>+</sup>	PreQ <sub>1</sub>	Lra WT <sup>b</sup> (77, with 5'P1)	[43]
II	<i>Spn</i>	NMR	2MIY	(Ca <sup>2+</sup> , K <sup>+</sup> )	PreQ <sub>1</sub>	Spn WT (58)	[44]

<sup>a</sup> L2var changes are A13C14A15U16.

<sup>b</sup> P4 loop changed from AAA to UUCC.

the major groove and down to the G–C bp below, at the ‘floor’, and has van der Waals contacts with guanine N7 and O6 (Fig. 3B, D; see also Fig. 7) [45,51]. In the crystal structure of Tte WT the exocyclic amine is sterically occluded from interacting with G5 by a bound SO<sub>4</sub><sup>2-</sup> and is in the plane of the preQ<sub>1</sub> ring (Fig. 3F). However, substitution of G5 for diaminopurine, which replaces the keto group at position 6 with an amine, decreased the binding affinity more than 450-fold for preQ<sub>1</sub> and 46-fold for preQ<sub>0</sub>, indicating that the interaction between the methyl amine of preQ<sub>1</sub> and the O6 of G5 is also important for binding affinity in the Tte riboswitch despite the absence of interaction in the crystal structure [48].

In addition to the interaction of the preQ<sub>1</sub> methylamine to G5 in the ‘floor’ of the binding pocket, the base quartet and base triple below and above the binding core stabilize preQ<sub>1</sub> in the binding pocket by stacking interactions and also sterically occlude it from exiting except from the major groove side. The loop 2 adenine (A16 in *Bsu*, A14 in *Tte*) in the ‘ceiling’ A–G–C triple stacks on the loop 2 C that pairs with preQ<sub>1</sub>

(C17 in *Bsu*, C15 in *Tte*). However, an A at this position is only 30% conserved, and is instead a U in 70% of the sequences (Fig. 2A). A U–G–C triple would be nearly isosteric with the A–G–C triple (Fig. 3G), and could in fact be more stable by adding an additional hydrogen bond between the 2'OH of G and O4 of U.

### 3.2. Mechanism of transcriptional and translational regulation

In the seminal study of the *Bsu* riboswitch the aptamer domain and a terminator hairpin were identified, but no obvious mechanism for ligand dependent control of terminator formation was found [39]. The solved structures of the *Bsu* riboswitch immediately suggested the classic terminator–antiterminator switching mechanism of riboswitch transcriptional control, and an antiterminator was identified whose stem would sequester the 3'-end of the A-rich tail required for formation of the pseudoknot (Fig. 2C) [45,46]. For the *Bsu* riboswitch, the antiterminator is predicted to be significantly less stable than the

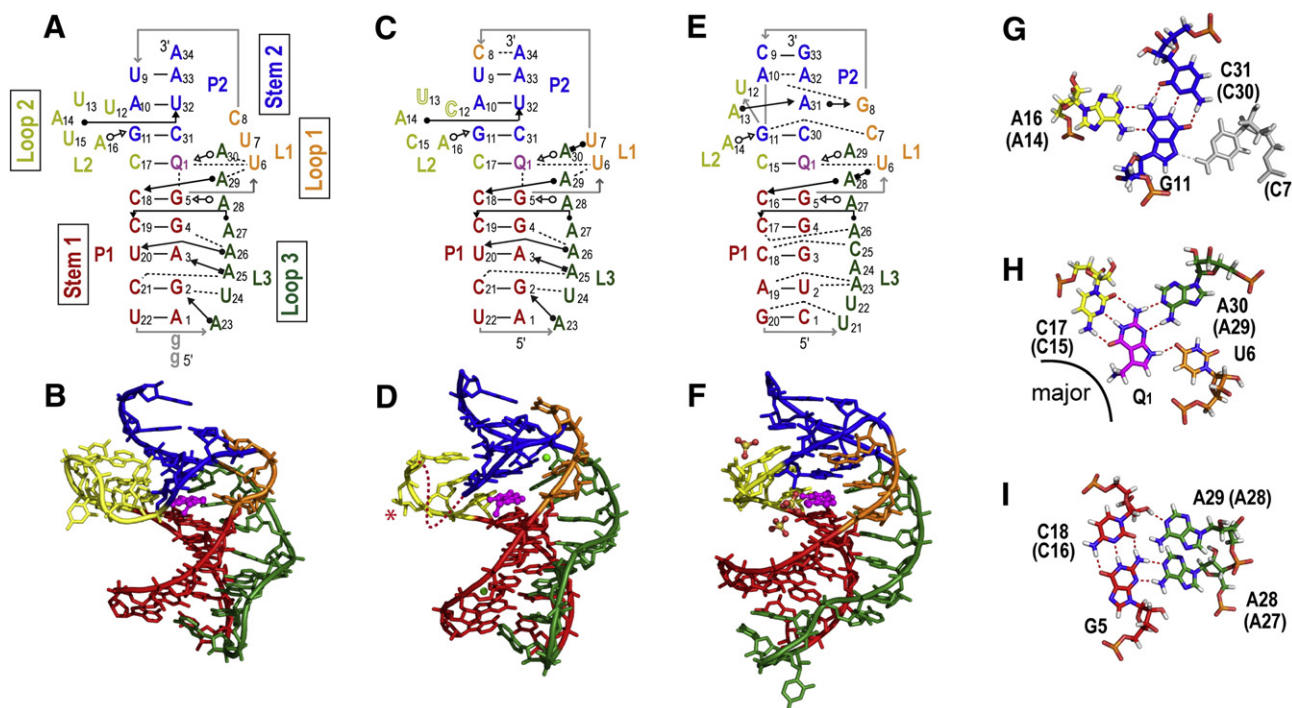


**Fig. 3.** Structures of preQ<sub>1</sub>-I riboswitch aptamers. (A–B) Solution NMR structure of *Bsu* (C12,15U) (PDB ID: 2L1V), (C–D) X-ray crystal structure of *Bsu* WT (PDB ID: 3FU2) and (E–F) X-ray crystal structure of *Tte* WT (PDB ID: 3Q50). (A,C,E) Schematics of secondary structures with base interactions illustrated using the symbols from Leontis and Westhof notation [87]. (B, D, F) Three-dimensional structures. Nucleotides C12 and U13 (shown as a dotted line) and the base of C15 (marked with an asterisk) are missing from the electron density in the *Bsu* WT crystal structure (D). Mg<sup>2+</sup> and SO<sub>4</sub><sup>2-</sup> are depicted as green, and yellow and red spheres, respectively. (G, H, I) Stick representation of the three layers of the preQ<sub>1</sub>-I binding pocket (from *Bsu* WT) showing (G) ‘ceiling’: loop 1–stem 2 A–G–C triple (A–G–C–C quartet for *Tte*, the loop 1 C shown in gray). (H) ‘Binding core’: preQ<sub>1</sub>–loop 2–loop 3–loop 1 preQ<sub>1</sub>–C–A–U quartet, and (I) ‘floor’: loop 3–stem 1–loop 3 A–C–G–A quartet. The corresponding residue numbers for *Tte* WT are given in parentheses. For all structures, residues are colored as follows: P1 (red), P2 (dark blue), L1 (orange), L2 (gold), L3 (green), and preQ<sub>1</sub> (magenta). For the preQ<sub>1</sub> binding core, hydrogen is white, nitrogen is blue, oxygen is red, phosphorus is orange, and carbon follows the main color scheme. For ease of comparison, structures are numbered starting with the first nucleotide in P1; note that this differs by two from the numbering used for the NMR structure of *Bsu* aptamer in references [45,50].

terminator. NMR studies of a 52 nt RNA construct containing the aptamer and anti-terminator sequence (but not the terminator) confirmed formation of the antiterminator in the absence of preQ<sub>1</sub>, and showed that when the antiterminator is present preQ<sub>1</sub> addition did not induce the pseudoknot to form [45]. An <sup>19</sup>F NMR study of a selectively labeled full-length transcriptional *Fnu* riboswitch found that in the absence of preQ<sub>1</sub> the expression platform had a 50:50 distribution between anti-terminator and terminator, which have comparable stabilities [52]. In this case, addition of preQ<sub>1</sub> shifted the equilibrium to 80% terminator. This is in contrast to several other transcriptional riboswitches, where addition of ligand to the full-length riboswitch does not cause a response *in vitro* [53,54].

The structure of the Tte riboswitch bound to preQ<sub>0</sub> [47] or preQ<sub>1</sub> [48] also suggested a translational control mechanism, where the 5' end of the SD sequence is sequestered as part of P3 (stem 2 of H-type pseudoknot) of the folded aptamer. However, only the first two residues of the SD sequence are paired, at the top of P3 (Fig. 3E).

### 3.3. Comparison to preQ<sub>1</sub>-I riboswitch preQ<sub>0</sub> bound and apo structures

Three structures of the *Tte* riboswitch have been determined: with preQ<sub>0</sub> bound [49], with preQ<sub>1</sub> bound, and the “apo” form without ligand [48]. The preQ<sub>0</sub> and preQ<sub>1</sub> bound aptamer structures are almost identical, with an RMSD of 0.578 Å, including the position of the ligands (Figs. 3H, 4F). Improved affinity (5–10 fold) and selectivity for preQ<sub>1</sub> vs preQ<sub>0</sub> are apparently conferred by the additional van der Waals or electrostatic interactions between the exocyclic amine of preQ<sub>1</sub> and the base pair below the preQ<sub>1</sub>-quartet, at the floor of the binding pocket.

There are only a few structures of ligand-free riboswitch aptamers [55]. The structure of the Tte translation-regulating riboswitch in the absence of preQ<sub>1</sub> revealed a pre-organized binding pocket with high similarity to the bound conformation (1.7 Å overall RMSD) [48]. Intriguingly, loop 2 residue A14 occupies the position of preQ<sub>1</sub> in the preQ<sub>1</sub>-bound structure where it interacts with A29 (loop 3) and U6 (loop 1), while loop 2 residue C15, which forms a WC bp with preQ<sub>1</sub> in the preQ<sub>1</sub> bound structure, is flipped out (Fig. 4C). The position of A14 in the binding core disrupts the stacking of the loop 2 bases next to stem 2 (Fig. 4B). The authors propose that this makes the last two residues of stem 2, A32G33, at the beginning of the Shine–Delgarno (SD) sequence more accessible to the 16S rRNA of the ribosome.

### 3.4. Cation interactions in preQ<sub>1</sub>-I aptamers

Due to the close approach of phosphates from tertiary interactions in pseudoknots, they are in general stabilized by divalent cations. Many riboswitch pseudoknots also require divalent cations as a prerequisite for ligand binding [56–60]. The NMR structure of the Bsu preQ<sub>1</sub>-I riboswitch was determined in 50 mM KCl, without added divalent cations, indicating that the aptamer can fold and bind preQ<sub>1</sub> tightly in the absence of divalent cations. The NMR study of an *Fnu* preQ<sub>1</sub>-I riboswitch also showed evidence for pseudoknot formation with preQ<sub>1</sub> without Mg<sup>2+</sup>, but Mg<sup>2+</sup> was apparently required for all molecules to fold [49,61]. In the crystal structures of Bsu WT and Bsu L2var, two to five Ca<sup>2+</sup> are present in different molecules of the asymmetric unit, but only one, located at the sharp turn in the backbone between U7 and C8 is shared in common among the crystal forms. A second Ca<sup>2+</sup>, visible only in the higher resolution Bsu L2var structure, interacts with the preQ<sub>1</sub> amino methyl group via a Ca<sup>2+</sup> hydration water and was proposed to contribute to ligand binding [46]. To investigate the effect of Ca<sup>2+</sup> on the preQ<sub>1</sub>-I Bsu aptamer structure, Zhang et al. [50] compared the solution and crystal structures of the preQ<sub>1</sub>-I Bsu aptamer in the presence and absence of Ca<sup>2+</sup> using NMR order tensor analysis of RDCs. This analysis indicated that in the presence of Ca<sup>2+</sup> the solution structure of the preQ<sub>1</sub> bound Bsu C12,15U riboswitch becomes more similar to the crystal structure. Analysis of chemical shift changes during titration of Ca<sup>2+</sup> revealed one higher affinity binding Ca<sup>2+</sup> with an

apparent K<sub>d</sub> of 47 μM located near the tight turn and a second weaker Ca<sup>2+</sup> binding site likely corresponding to the one near the preQ<sub>1</sub> methylamine in the Bsu L2var crystal structure [50]. NMR relaxation studies also showed that loop 1 residues U7 and C8 are dynamic in solution without Ca<sup>2+</sup>, but that conformational exchange of C8 on the slow timescale (μs–ms) is completely quenched upon Ca<sup>2+</sup> binding (Fig. 5A) [50].

The crystal structures of preQ<sub>1</sub>- and preQ<sub>0</sub>-bound translation-regulating Tte riboswitches also did not contain any ordered divalent cations, although MgCl<sub>2</sub> was present in the crystallization buffer. Instead, they both contain 4 SO<sub>4</sub><sup>2-</sup> ions, two of which stabilize C16 and C18 in stem 1 by coordinating to the C amino group. In the apo Tte preQ<sub>1</sub>-I riboswitch, one Mg<sup>2+</sup> coordinates to N7 of G5 at the top of P1. Taken together, these results indicate that divalent cations stabilize but are not required for preQ<sub>1</sub> binding in preQ<sub>1</sub>-I riboswitches.

### 3.5. PreQ<sub>1</sub>-I riboswitch folding and dynamics

#### 3.5.1. SAXS and computational studies of folding of the translation-regulating Tte riboswitch

Given that the solution NMR data indicated that the preQ<sub>1</sub>-I aptamer requires preQ<sub>1</sub> for pseudoknot formation [45,49], the structure of the compact apo Tte riboswitch was somewhat surprising (Fig. 4A–C). In the apo form, A14 rearranges to occupy the preQ<sub>1</sub> site, as discussed in Section 3.3. This rearrangement collapses the “ceiling” of the binding pocket, increasing the solvent accessibility of the SD sequence nearly 50 Å<sup>2</sup>, coupled with a 7.6% increase in unit cell volume [48]. The increased exposure of the SD may explain how the Tte riboswitch can regulate translation in the absence of preQ<sub>1</sub>. Wedekind and coworkers [48] also performed SAXS experiments, which provided evidence that the compact structure of the apo riboswitch seen in the crystal structure is also present in solution. However, deviations were observed when the SAXS scattering profile was compared to the crystallographic coordinates, indicating that in solution there likely exists an ensemble of ‘open’ and ‘closed’ states. Single molecule Förster Resonance Energy Transfer (smFRET) and computational studies by Suddala et al. [62] on the Tte riboswitch showed that, consistent with the SAXS data, in the absence of preQ<sub>1</sub> the Tte riboswitch dynamically samples two states: a mid-FRET state, which is a diverse ensemble of partially folded conformations, and a high-FRET state, which is consistent with the folded apo Tte structure (Fig. 4A). Molecular dynamics simulations by Banas et al. [63] of the Tte preQ<sub>1</sub>-I riboswitch revealed that the relatively short P2 stem of the apo structure was highly unstable and irreversibly melted on the μs timescale while the P2 stem of the bound structure was stable. The stability of P2 appeared to be dependent upon stacking interactions between the terminal U10–A32 bp and L2 residue A13. In the absence of preQ<sub>1</sub>, L2 showed conformational plasticity in contrast to the bound Tte structure, whose L2 conformation remained stable. This study concluded that loop 2 could act as a sensor for ligand by providing different stacking arrangements for P2 and modulating its stability [63].

The Tte apo conformation may allow for faster ligand recognition by weakly forming the binding pocket, A-minor interactions, and pseudoknot contacts, allowing preQ<sub>1</sub> to quickly enter the binding pocket and lock the pseudoknot in place. The ability of the Tte riboswitch to undergo exchange between a compact partially folded and bound-like conformation agrees with the notion that transcription-regulating riboswitches are kinetically controlled whereas translation-regulating riboswitches are thermodynamically controlled, in which the aptamer exists in equilibrium between open and closed states that is shifted to the bound state on binding ligand. It is worth noting that *Tte* is a thermophilic organism, ideally growing at 75 °C, and the equilibrium between open and closed states is likely to be shifted toward the former at that temperature. Suddala et al. [62] tested the temperature dependence of preQ<sub>1</sub> binding for the Tte riboswitch, and found that the K<sub>d</sub> was reduced ~60 fold from 25 °C to 60 °C, to 430 nM, in support of this hypothesis.

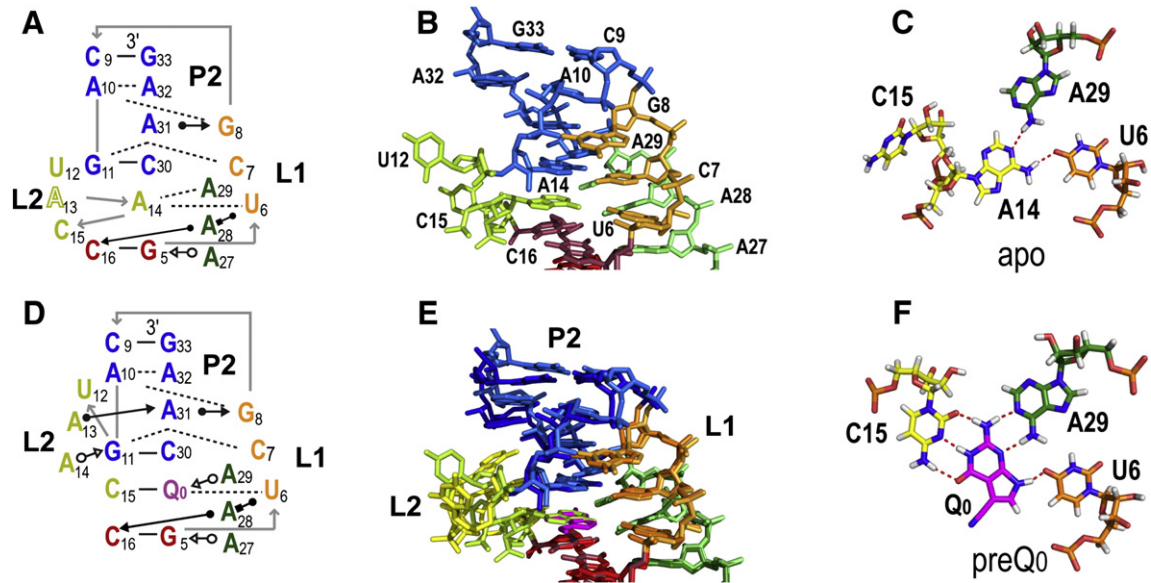


**Fig. 4.** X-ray crystal structures of the apo and preQ<sub>0</sub> bound Tte preQ<sub>1</sub>-I riboswitch. (A–C) Apo Tte WT: (A) Schematic of secondary structures and base interactions at and above preQ<sub>1</sub> binding pocket. (B) Stick representation of structure of the regions shown in (A). (C) The loop 2–loop 3–loop 1 A14–A29–U6 base triple formed in the apo structure, where A14 replaces preQ<sub>0</sub> or preQ<sub>1</sub> in the binding core. C15 is flipped out of the binding pocket. (D–F) Tte WT with preQ<sub>0</sub>: (D) Schematic of secondary structure at and above preQ<sub>1</sub> binding pocket. (E) Superposition of the apo and preQ<sub>0</sub> bound structures, to highlight the similarities and differences. (F) The preQ<sub>0</sub>–loop 2–loop 3–loop 1 preQ<sub>0</sub>–C15–A29–U6 quartet.

### 3.5.2. Biophysical studies of folding of transcription-regulating riboswitches

Given the very small size of the aptamer, the preQ<sub>1</sub>-I riboswitch posed a challenge in understanding how it could function within the timeframe of transcription. Early NMR studies and SAXS data [45,48,49] suggested that unlike the Tte translation-regulating riboswitch, the transcription-regulating Bsu and Fnu riboswitches do not form the pseudoknot in the absence of ligand. In the NMR construct of the Bsu riboswitch, the two additional Gs at the 5' end of the Bsu NMR result in the formation of a more stable alternate P1A helix in the absence of preQ<sub>1</sub> (Fig. 5B). This hairpin occludes U6 and C17 that participate in the binding core, preventing formation of the ligand binding pocket. In the full-length riboswitch, P0, located 0–2 nt upstream from P1, may act to prevent incorrect (P1A) hairpin formation during co-transcriptional

folding (Fig. 2C). For the Fnu riboswitch, Micura and coworkers [64] showed that the riboswitch aptamer forms a dimer at a palindromic sequence within the apical loop overlapping with the P2 site, preventing pseudoknot formation (Fig. 5C). This dimer, which is unlikely to be relevant in vivo, would explain the relatively large radius of gyration observed in the SAXS data [48]. By using a construct with a base pair substitution in P2 to prevent dimer formation, the authors found NMR evidence that stem 2 of the pseudoknot could form in the absence of ligand in a temperature and/or Mg<sup>2+</sup> dependent fashion [64]. This mutant Fnu riboswitch that reduced dimerization had a two-fold higher observed K<sub>d</sub> [49], although it should be noted that this mutation swapped an A–U bp in P2 to a G–C bp thereby increasing the thermostability of P2, which may explain the observed prevalence of pseudoknot formed in the absence

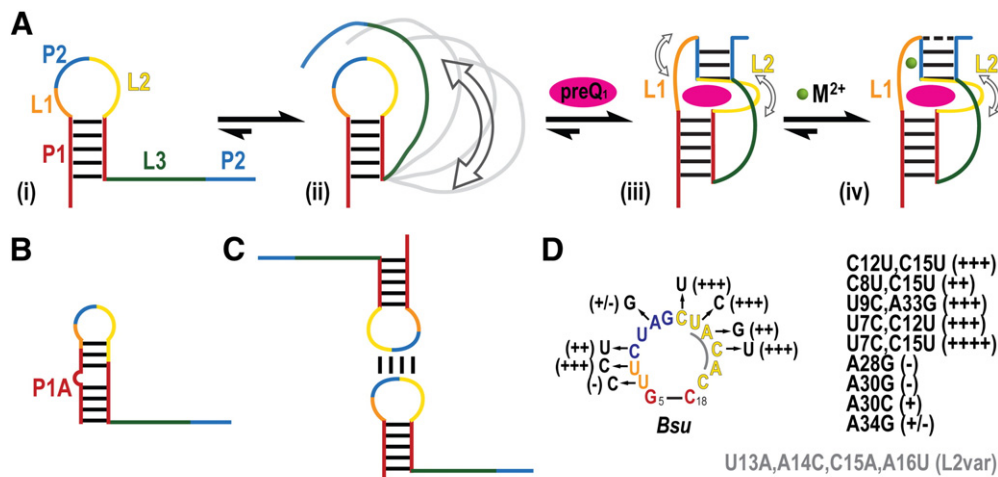


**Fig. 5.** Schematic of preQ<sub>1</sub>-I riboswitch folding pathway. (A) (i) The Bsu riboswitch initially folds into a hairpin followed by a flexible ssRNA tail. (ii) The ssRNA tail, in the presence of divalent cations, dynamically samples a variety of conformations (illustrated in gray), some of which bring L3 close to P1. (iii) On addition of preQ<sub>1</sub>, the P2 stem forms and L3 docks into the P1 minor groove. L1 and L2 show dynamics on the  $\mu$ s–ms and ps–ns timescales, respectively (open arrows). (iv) Divalent cations bind to L1, quenching local flexibility while retaining L2 motions. (B) Alternate P1A hairpin observed in Bsu NMR construct as a result of additional 5' GG residues. (C) A palindromic sequence commonly observed overlapping with the P2 site in the P1 loop gives rise to dimers. (D) Effect of Bsu loop mutagenesis on apparent preQ<sub>1</sub> binding. +++ better than WT, ++ equivalent to WT, + and +/- worse than WT, – no detectable binding. Multiple mutations or mutations to L3 are inset. Mutations in Bsu L2var are shown in gray.

of preQ<sub>1</sub> (relative to WT) and the modest improvement in binding affinity. Additional fluorescence studies on the Fnu WT at low concentrations showed that the on-rate for preQ<sub>1</sub>-binding in the Fnu riboswitch was extremely fast compared to other transcription-regulating riboswitches [52].

The WT Bsu riboswitch was also observed to form dimers by NMR and electrophoretic mobility shift assays, similar to the Fnu riboswitch [62,65] (Fig. 5C). The Bsu C12,15U construct used to solve the NMR solution structure, which disrupts the palindromic sequence and prevents dimer formation, had better NMR spectra and required less preQ<sub>1</sub> to saturate binding than the WT sequence [45] (Fig. 5D). Kang et al. made multiple substitutions to L2 for their NMR study (Fig. 5D). Analysis of their results on preQ<sub>1</sub> binding reveals that mutations that would disrupt dimer formation improved the apparent binding affinity for preQ<sub>1</sub>, as judged by NMR titrations (Fig. 5D). The ability to modify L2 with no apparent loss in preQ<sub>1</sub> recognition is consistent with its low sequence conservation, indicating that the sequence identity is not important but rather its length and flexibility, as discussed below. Unlike the Fnu riboswitch, the NMR studies of the Bsu riboswitch showed no sign of pseudoknot formation in the absence of preQ<sub>1</sub> even in the Bsu C12,15U construct that does not form dimers [45,65]. However, smFRET studies by Walter and co-workers [62] showed that in the presence of Mg<sup>2+</sup>, the Bsu WT riboswitch adopts a compact conformation in the absence of preQ<sub>1</sub>. Although the absence of divalent cations could contribute partially to the unfolded conformation observed in the NMR study, it is also likely that the alternate P1A hairpin would prevent stable pseudoknot formation, as discussed above. The smFRET studies also provided evidence that the Bsu riboswitch transiently forms a compact conformation that brings the 3' ssRNA tail close to the P1 apical loop at primarily <100 ms timescales. An additional explanation for the discrepancy between smFRET and NMR data is that the timescale of the transition between unfolded and partially folded conformations occurs outside the window of detection by NMR. For example, transient, lowly populated interactions of the 3' tail with the P1 stem on the  $\mu$ s to low ms timescales would be invisible by NMR. A combined NMR and computational study on the Bsu preQ<sub>1</sub>-I riboswitch 12 nt 3' tail revealed that the A-rich tail contains a surprising degree of order, adopting an A-form-like conformation on average [65]. This partial ordering may facilitate rapid ligand recognition by reducing the conformational entropy of the single strand, docking the tail into the P1 minor groove on preQ<sub>1</sub> capture.

Comparing the smFRET studies of the Tte and Bsu riboswitch, Walter and coworkers [62] found that the Tte riboswitch exhibits much slower “switching” than the Bsu riboswitch. To obtain insights into the folding and ligand-binding pathway, Gō model molecular dynamics simulations were performed for both riboswitches. An earlier computational study posited that the Bsu aptamer folded in a concerted manner, with the P1 stem forming first, followed by A-minor interactions, preQ<sub>1</sub> recognition, and P2 formation occurring nearly concomitantly [66]. In contrast, the Tte riboswitch appears to have significantly different folding behavior: P1 forms first, quickly followed by preQ<sub>1</sub> binding, with A-minor interactions and P2 formation happening much later in the simulation [62]. It should be noted that Gō model simulations begin with an extended RNA chain and bias the simulation toward the fully folded state bound to ligand; therefore, it is unlikely that the experimentally determined apo structure will be observed under such conditions. Similar results were obtained from an independent computational study by Gong et al. [67] using high-temperature unfolding simulations of the Tte and Bsu aptamers.

Zhang et al. [50] investigated the flexibility of loops 1 and 2 of preQ<sub>1</sub>-bound Bsu C12,15U using NMR <sup>13</sup>C relaxation dispersion studies. U12, U13, and U15 are highly flexible, consistent with their extruded conformation, while A14, A16, and C17, which are stacked on each other in the minor groove of P2, have limited mobility. In the crystal structures of the Bsu riboswitch, L2 nts C12, U13 and the base of C15 in Bsu WT and most of L2 (U13–A16) in Bsu L2var had missing electron density, providing

independent evidence for flexibility of L2 [46]. While L2 was found to have fast motions occurring on the ps–ns timescale, L1 residues U7, C8, and U9 have slower motions on the  $\mu$ s–ms timescale. Interestingly, C8 motions are quenched on addition of Ca<sup>2+</sup> with concomitant changes to the L1 conformation, as described above in Section 3.4. The authors conclude that L1, aided by divalent cations, effectively functions as a ‘lid’ to block preQ<sub>1</sub> exit upon ligand capture.

Together, these data paint a picture of the pathway of preQ<sub>1</sub> recognition (Fig. 5A). By modulating variables peripheral to the binding core such as the length of L2, the thermostability of P2, and the degree of order in loop 3 to allow rapid docking on ligand recognition, the preQ<sub>1</sub>-I riboswitch can tune its responsiveness to intracellular conditions. Variations in loop 2 sequence and length can modulate preQ<sub>1</sub> binding affinity and pseudoknot stability while the loop 3 sequence may influence kinetics of ligand recognition [62,65]. Taken together, these studies suggest a general mechanism of ligand regulation wherein preQ<sub>1</sub>-I riboswitches utilize a dynamic loop 2 and unstable P2 stem to prevent premature pseudoknot formation and loop 1 (with aid of divalent cations) to block preQ<sub>1</sub> exit on capture.

### 3.5.3. Computational model studies

The small size of the minimal riboswitch aptamer (34 nt) lends itself well to computational studies as a model system for investigating the impact of small molecules on RNA stability. In one molecular dynamics study, Denning et al. [68] found that in the presence of the osmolyte trimethylamine N-oxide (TMAO) the bound Bsu crystal structure becomes destabilized due to dehydration of the phosphate backbone caused by interactions between the backbone and a protonated form of TMAO. In another molecular dynamics study, Yoon et al. [69] examined the mechanism of urea-induced denaturation of nucleic acids using the bound Bsu NMR structure and found that the two-step denaturation mechanism is the opposite of urea-induced unfolding of proteins.

## 4. The preQ<sub>1</sub>-II riboswitch

### 4.1. Structures of preQ<sub>1</sub>-II riboswitches

The aptamer domain of preQ<sub>1</sub>-II riboswitches is much larger (56 nt) than that of preQ<sub>1</sub>-I riboswitches (34 nt). All preQ<sub>1</sub>-II riboswitches identified to date regulate translation and contain a SD sequence at their 3' end (Fig. 2D) [40,42]. Formation of a pseudoknot by this riboswitch was easily predicted based on the high conservation of pyrimidine residues complementary to the SD sequence on the 3' side of the loop of the stem 1 (P2) hairpin (Fig. 2B). The preQ<sub>1</sub>-II riboswitch also contains a highly conserved unpaired C above the top of P1 that was hypothesized to form a WC bp to preQ<sub>1</sub> [42]. Although a C-to-U substitution reduced the binding affinity by two orders of magnitude, the ligand specificity did not change to favor adenine analogs as often occurs with purine riboswitches, suggesting that the preQ<sub>1</sub>-II riboswitch does not form a canonical WC bp with ligand.

Two structures of preQ<sub>1</sub>-II riboswitches have been determined, an X-ray crystal structure from *Lactobacillus rhamnosus* (*Lra*) containing 75 nt (*Lra* WT') [43] and subsequently an NMR solution structure from *Streptococcus pneumoniae* (*Spn*) containing 59 nt (*Spn* WT') [44]. The *Lra* WT' includes the hairpin preceding the folded aptamer domain, which by published convention is called P1, so for these riboswitches stem 1 is called P2 and stem 2 is called P3 (Fig. 6). In the crystal structure, P1 stacks on the bottom of P2 but does not contribute to ligand binding. Excluding the single strand residues at the 5' and/or 3' ends, both aptamer domains are 56 nt long, but have different sequences.

The preQ<sub>1</sub>-II riboswitches form an unusual H-type pseudoknot with a hairpin embedded in loop 3, which is classified as HL<sub>out</sub> [70]. The pseudoknot has an 8–9 bp stem 1 (P2) and 6 bp stem 2 (P3). Loop 1 is 5 nt, loop 2 is a single nt, and loop 3 is 19–22 nt, including the embedded hairpin (P4) of 4 bp capped by a tetraloop (Fig. 6A, C). Although both the

preQ<sub>1</sub>-I and preQ<sub>1</sub>-II riboswitch aptamers form pseudoknots, their overall architecture and mode of sequence recognition are very different (Figs. 6 and 7). Loop 1 (J2–3) interacts in the major groove of stem 1 (P2), with the first C forming a non-canonical bp with preQ<sub>1</sub> and the next two Us interacting with the two A–U bps at the bottom of stem 2 to form two U–A–U triples. This triple helical region is similar to that seen in the human telomerase RNA pseudoknot [71]. Since the SD sequence AAGGAGA forms one strand of stem 2 (P3), the two Us from loop 1 and two Us from stem 2 form a ‘U-trap’ [72] that sequesters the SD sequence and stabilizes the preQ<sub>1</sub> binding pocket (Fig. 6A, C). This explains the highly conserved Us on either side of the stem 1 hairpin loop in the preQ<sub>1</sub>-II riboswitch (Fig. 2B). As in the preQ<sub>1</sub>-I riboswitches, preQ<sub>1</sub> inserts at the junction between stem 1 and stem 2 and forms a base pair with loop 2, but in this case loop 2 is a single U nt, rather than the unusually long loop 2 in preQ<sub>1</sub>-I riboswitches. The most unusual feature of the preQ<sub>1</sub>-II pseudoknot is the long loop 3 with its embedded P4 hairpin. The single strand nucleotides 5′ to P4 in J2–4 (7 nts in Spn and 4 nts in Lra) do not interact with the minor groove as in the preQ<sub>1</sub>-I and almost all other H-type pseudoknots, but rather span across the major groove without any contact to the bases of stem 1 (Fig. 8C–D). P4 is extended by two nts on each side (extended P4) and forms a three-way junction with stem 1 and stem 2 (Fig. 6A, C). Adenines on either side of the extended P4 form interactions in the binding pocket.

A major difference in the solved structures of the Spn WT and Lra WT′ preQ<sub>1</sub>-II riboswitches is the position of P4 (Fig. 6B, D). In the crystal structure of Lra WT′, P4 is bent at a 98° angle relative to the rigid P2–P3 stem, while in the lowest energy NMR structure of Spn WT P4 is bent at a 77° angle relative to the P2–P3 stem. However, NMR dynamics measurements [44] and FRET studies [73] indicate that the position of P4 in the Spn riboswitch in solution is dynamic (Fig. 6E), as discussed in Section 4.3. Most preQ<sub>1</sub>-II riboswitches have 7 bps in P2 and 9 or more nts in J2–4. The Lra riboswitches are an exception, with a longer 8–9 bp P2 and shorter 6–7 nt J2–4 [40]. The differences in the lengths of P2 and J2–4 between Lra WT′ and Spn WT might result in the different position of P4 in the crystal and NMR structures, but it is also possible that in solution P4 of Lra WT′ is dynamic. P4 has been proposed to play a major role in how the riboswitch regulates translation, preventing stable formation of the pseudoknot in the absence of preQ<sub>1</sub> [44,73], as discussed in Section 4.3.

#### 4.1.1. The preQ<sub>1</sub>-II binding pocket

PreQ<sub>1</sub> is stabilized in the binding pocket (Fig. 7F) by hydrogen bond and van der Waals interactions that form a base quartet in the binding core (Figs. 6F, 7D), a base quartet above (Fig. 7E), and a base pair below preQ<sub>1</sub> (Fig. 7F). In the binding core, specificity for preQ<sub>1</sub> is achieved from hydrogen bonding to a C residue from loop 1 (C8 in Spn, C30 in Lra) and the U residue that comprises loop 2 (U19 in Spn, U41 in Lra) and by van der Waals interactions to the last residue of loop 3 which is an A (A50 in Spn, A70 in Lra) (Fig. 7D). Although preQ<sub>1</sub> is also recognized by C, A, and U residues from each of the three loops in the preQ<sub>1</sub>-I riboswitches, the C and U are on different loops and the interactions of all three nucleotides differ between the two classes (Fig. 7A, D). The C–preQ<sub>1</sub> interaction is an unusual *trans* WC/WC bp, in contrast to the *cis* WC/WC bp of the C–preQ<sub>1</sub> interaction in preQ<sub>1</sub>-I riboswitch (Fig. 7A, D). The loop 2 U has 3 hydrogen bonds to the ‘sugar’ edge of preQ<sub>1</sub> (N2H, N3, and N9H). The interaction of preQ<sub>1</sub> with the loop 3 A (A50 in Spn) is unusual in that specificity is achieved by van der Waals contacts rather than hydrogen bonds; the loop 3 A has a single hydrogen bond to the loop 2 U 2′OH, but its base and ribose C1′/H1′ and 2′O pack tightly along the N9H–C8H–methylene edge of preQ<sub>1</sub> (Figs. 6F, 7D). The van der Waals interactions between the preQ<sub>1</sub> exocyclic methylene group and A50 2′O explain the > 100 fold lower binding affinity for 7-carboxamide-7-deazaguanine, which has a carbonyl group at that position [42]. In contrast, there is almost no decrease in binding affinity to the preQ<sub>1</sub>-I riboswitch, where the preQ<sub>1</sub> methylene group does not have any specific interactions with the neighboring

residues and there is enough room to accommodate a carbonyl group (Fig. 7A, C, D, F).

The bottom of the binding pocket, below the preQ<sub>1</sub> binding core, is a G–C bp in Spn and an A–G bp in Lra located at the top of stem 1. Unlike the case for the preQ<sub>1</sub>-I riboswitch, there is no specific interaction between the preQ<sub>1</sub> exocyclic amine group and the bottom of the binding pocket, perhaps explaining the observed sequence variability. Instead of pointing down toward the base pair below, the exocyclic methylamine points up, with possible interactions with O2 of U9 or the phosphate backbone of A51 (Fig. 7C, F). Above the preQ<sub>1</sub> binding core, there are two loop 1–stem 2 U–A–U triples that stabilize the binding pocket. The bottom triple, which forms the top of the binding pocket, has an additional interaction with a loop 3 A (A35 in Spn, A55 in Lra) to form a loop 1–stem 2–loop 3 U–A–U–A base quartet (Fig. 7E). This A is at the 5′ end of the extended P4 helix and forms an A-minor interaction with the stem 2 A 2′OH (A51 in Spn, A71 in Lra). The extended P4 positions the adenines at either end (A35 and A50 in Spn) to interact with the top and core of the binding pocket (Fig. 7E, F) by a rotation of the P4 helix about its axis (Fig. 6E). One of the most significant differences between the preQ<sub>1</sub>-I and preQ<sub>1</sub>-II binding pockets is that for the former preQ<sub>1</sub> enters from the major groove side, with only its exocyclic amine exposed to solvent, while for the latter preQ<sub>1</sub> enters from the minor groove side (Figs. 7 and 8).

#### 4.2. Cation interactions in the preQ<sub>1</sub>-II aptamers

Unlike the preQ<sub>1</sub>-I riboswitch, the preQ<sub>1</sub>-II riboswitch requires divalent cations for high affinity binding [43,44]. The NMR solution structure of Spn WT was solved in the presence of Ca<sup>2+</sup> and the crystal structure of Lra WT contained both Mg<sup>2+</sup> and Cs<sup>+</sup>. In the Lra WT crystal structure, two Mg<sup>2+</sup> are bound to the backbone of the G at the top of P2 and the C in loop 1 that recognizes preQ<sub>1</sub>, in the three-way junction between stems P2, P3, and P4. Several Cs<sup>+</sup> and one Mg<sup>2+</sup> are located in J2–4, the P4 stem, and at the bottom of P2, potentially stabilizing J2–4:P2 and J2–4:P4 interactions. ITC measurements indicated that addition of Mg<sup>2+</sup> or Ca<sup>2+</sup> increases the binding affinity of preQ<sub>1</sub> by 100-fold [44]. Based on chemical shift changes of residues near the binding pocket when Ca<sup>2+</sup> was added in the presence of preQ<sub>1</sub>, the authors propose that divalent cations stabilize the base triples and the position of A35 and A50 in the binding pocket. A smaller divalent cation effect for preQ<sub>1</sub> binding (4 fold) was observed for the Lra riboswitch [43], possibly due to its shorter J2–4.

The effect of divalent cations on the apo Spn riboswitch was also investigated using FRET, and the authors concluded that they stabilize formation of P3 in the pseudoknot [73]. NMR studies, which can give residue-specific interactions, indicate that in the absence of preQ<sub>1</sub> divalent cations only stabilize formation of the top half of P3 and not the base triples at and above the binding pocket [44].

#### 4.3. PreQ<sub>1</sub>-II riboswitch folding and dynamics

The preQ<sub>1</sub>-II riboswitch is less well-characterized than the preQ<sub>1</sub>-I riboswitch, despite being discovered around the same time. Micura and coworkers [73] performed SHAPE experiments over a range of temperatures to determine residue-specific melting of the Spn preQ<sub>1</sub>-II riboswitch in the free and preQ<sub>1</sub>-bound states. The authors found that in all cases J2–4 had a high degree of reactivity relative to helical elements, indicating flexibility within this loop. NMR <sup>13</sup>C spin relaxation measurements independently determined that this loop was highly dynamic [44]. smFRET studies showed that, similar to what was observed for the preQ<sub>1</sub>-I riboswitch, formation of the pseudoknot in the absence of preQ<sub>1</sub> is Mg<sup>2+</sup>-dependent for the Spn riboswitch. Deletion of the P4 stem in loop 3 (residues 38–48) slightly increased the stability of stem 2 in the absence of ligand and decreased the binding affinity for preQ<sub>1</sub> ~10-fold. Interestingly, the lifetime of the high-FRET state (where stem 2 was formed) was significantly shorter than the WT construct,

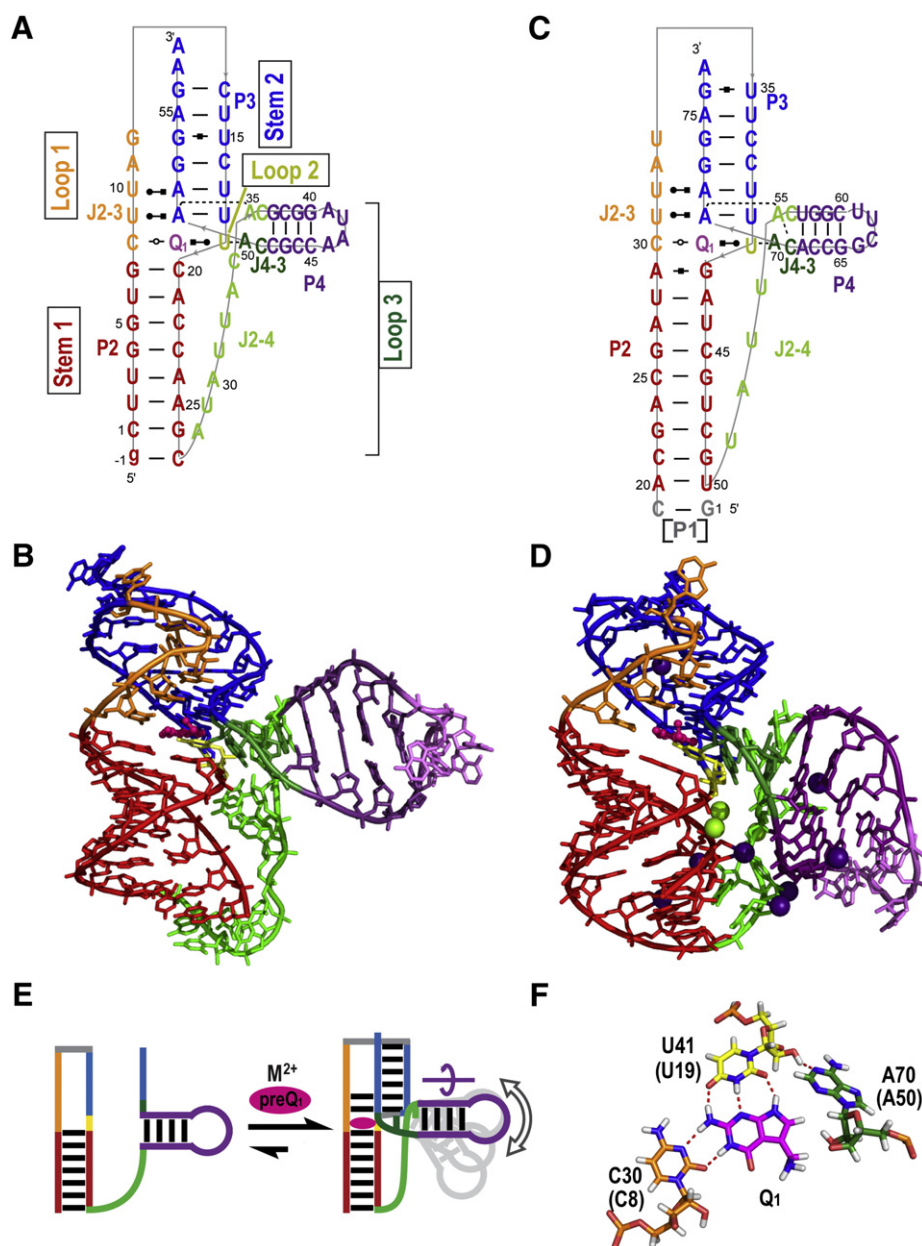


**Fig. 6.** Structures of preQ<sub>1</sub>-II riboswitches. (A–B) Solution NMR structure of Spn WT (PDB ID: 2MIY), (C–D) X-ray crystal structure of Lra WT' (PDB ID: 4JF2). (A, C) Schematics of secondary structures and base interactions. (B, D) Stick representation of three-dimensional structures. Mg<sup>2+</sup> and Cs<sup>+</sup> are depicted as green and purple spheres, respectively. (E) Schematic illustrating the secondary structure of the Spn riboswitch in the absence of preQ<sub>1</sub> and the divalent cation and preQ<sub>1</sub> induced folding. The curved arrow above P4 indicates the rotation of P4 required to position the two As (dark and light green bars) in the binding pocket. The gray P4 hairpins illustrate that the position of P4 is dynamic. (F) Stick representations of interactions of preQ<sub>1</sub> in the binding core showing the preQ<sub>1</sub>-loop 1-loop 2-loop 3 preQ<sub>1</sub>-C-U-A quartet from Lra WT'. For all structures, residues are colored as follows: P2 (red), P3 (dark blue), L1 (orange), L2 (gold), L3 (green, with P4 hairpin insert in purple), and preQ<sub>1</sub> (magenta). Note that P2 is stem 1 and P3 is stem 2 in standard H-type pseudoknot nomenclature.

particularly in the presence of preQ<sub>1</sub>, suggesting that although P4 deletion stabilizes the pseudoknot it reduces the ability of the riboswitch to stably bind preQ<sub>1</sub> [73]. Further, the P4 helix appears to have a high degree of flexibility even in the preQ<sub>1</sub>-bound state. smFRET experiments with fluorophores placed at L1 and P4 in the WT construct showed that the preQ<sub>1</sub>-bound structure falls approximately equally into two distributions: one in which the P4 helix is at an intermediate distance from L1 and one in which P4 is far from L1.

The NMR study of the Spn riboswitch by Kang et al. [44] indicated that P2 and P4 form in the absence of preQ<sub>1</sub> and Ca<sup>2+</sup> (Fig. 6E). As discussed in Section 4.2, in the presence of Ca<sup>2+</sup>, NMR spectra of apo Spn WT show imino proton resonances for the top part of P3 (3 bp), indicating that the pseudoknot is partially formed in agreement with smFRET data [73]. Deletion of the P4 stem (residues 36–49) (Spn ΔP4)

results in a reduction in binding affinity as measured by ITC similar to that observed in the smFRET study. Examination of imino proton spectra of apo Spn ΔP4 with Ca<sup>2+</sup> showed that the P3 stem is significantly stabilized in the absence of preQ<sub>1</sub>, with five of the six base pairs observed. Analyses of NMR RDC measurements and <sup>13</sup>C spin relaxation measurements are also consistent with the P4 dynamics observed in the smFRET study, revealing positional flexibility in P4 relative to a rigid P2–P3 (stem 1–stem 2) stem, corresponding to a 35° cone angle of motion about the P4 helical axis. This large motional amplitude would explain the ~20° difference observed in the P2–P4 inter-helical bend angle between Lra and Spn structures.

Taken together, the smFRET and NMR studies indicate that removing P4 reduces the range of motions accessible to loop 3, thereby increasing the likelihood to form the stem 2 of the pseudoknot. The P4 hairpin is a

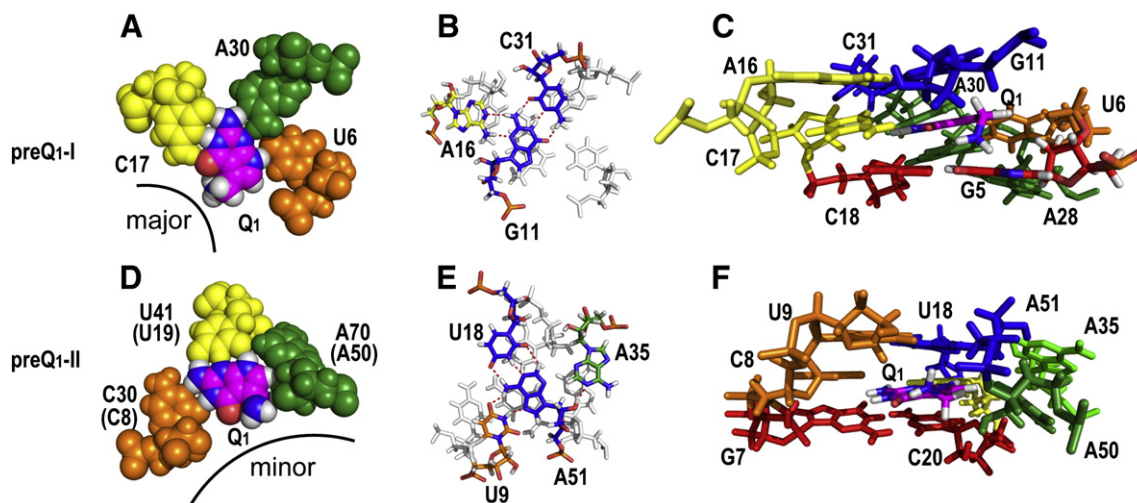


**Fig. 7.** The preQ<sub>1</sub> binding pocket for preQ<sub>1</sub>-I and preQ<sub>1</sub>-II riboswitch aptamers. (A–C) PreQ<sub>1</sub>-I structures of Bsu WT X-ray (A) and Bsu (C12,15U) NMR (B–C) and (D–F) preQ<sub>1</sub>-II structures of *Lra* WT crystal (D) and Spn WT NMR (E–F), comparing the preQ<sub>1</sub>-I and preQ<sub>1</sub>-II binding cores (A,D), ceiling of the binding pockets (B,E), and binding pockets (C,F). (A,D) Sphere representation of Bsu WT preQ<sub>1</sub>-loop 2–loop 3–loop 1 preQ<sub>1</sub>-C–A–U quartet (A) and *Lra* WT preQ<sub>1</sub>-loop 1–loop 2–loop 3 preQ<sub>1</sub>-C–U–A quartet (D), illustrating hydrogen bond and van der Waals interactions, especially between A50–preQ<sub>1</sub> and A50–U19. The corresponding residue numbers for Spn WT are given in parentheses. The exocyclic methylamine projects from the major groove in preQ<sub>1</sub>-I and from the minor groove in preQ<sub>1</sub>-II riboswitches. (B,E) Overlay of Bsu loop 2–stem 2 A–G–C triple on preQ<sub>1</sub>-C–A–U quartet (B) and Spn loop 1–stem 2–loop 3 U–A–U–A quartet on preQ<sub>1</sub>-C–U–A quartet (E). PreQ<sub>1</sub> quartets are gray. (C,F) Stick representations of the three layers of binding pocket from Bsu (C) and Spn (F) NMR structures, with G–C bp below, preQ<sub>1</sub> binding core, and base triple or quartet above. The exocyclic amine protons point down toward the G–C pair below and have van der Waals contact with O6 and N7 of G5 (C), and point up toward the base quartet above, with possible interactions with O2 of U9 or phosphate backbone of A51 (F).

special feature of preQ<sub>1</sub>-II riboswitch and was proposed to play a dual role by Kang et al. [44] based on the experiments described above as well as NMR and ITC data on A35 and A50 substitutions. In the presence of preQ<sub>1</sub> and divalent cations (Section 4.2), P4 positions the adenines at the 5' and 3' ends of P4 (A35 and A50 in Spn) to interact with the top and core of the binding pocket (Figs. 6F, 7E, F). Thus, the extended P4 helix acts as a 'screw' cap, positioning A35 and A50 in the binding pocket and blocking off ligand exit from that side. In the absence of preQ<sub>1</sub>, P4 destabilizes P3 therefore hindering pseudoknot formation.

## 5. Applications

### 5.1. Translational control via $-1$ frameshifting

Riboswitches hold great potential in a number of biotechnology applications due to their ability to regulate gene expression in *cis* upon addition of a cognate ligand [74,75]. To date, preQ<sub>1</sub> riboswitches have only been used in one such application. Yu et al. [76] took advantage of the pseudoknot structure of the bound preQ<sub>1</sub>-I aptamer to

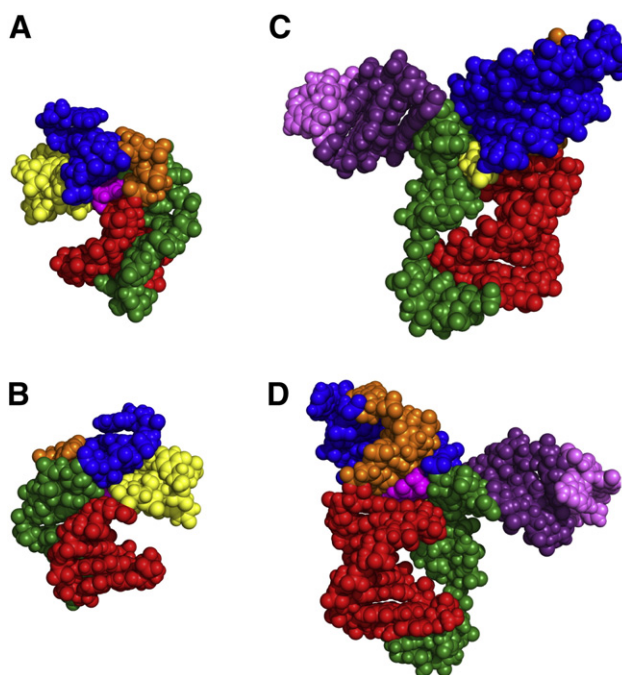


**Fig. 8.** Comparison of preQ<sub>1</sub>-II vs preQ<sub>1</sub>-I riboswitch structures. Sphere representation of (A,B) preQ<sub>1</sub>-I Bsu (C12,15U) and (C,D) preQ<sub>1</sub>-II Spn WT. (B, D) are the 180 degree rotation of (A, C), respectively. Loop 3 (green) lies along the minor groove in preQ<sub>1</sub>-I aptamers (A) while shows that loop 3 does not insert in a groove but spans the major groove in preQ<sub>1</sub>-II aptamers (B). The exocyclic amine group of preQ<sub>1</sub> projects out from the major groove of preQ<sub>1</sub>-I aptamers (A) and from the minor groove of preQ<sub>1</sub>-II aptamers.

induce  $-1$  ribosomal frameshifting in an in vitro translation assay. In the absence of preQ<sub>1</sub>, the transcription-regulating *Bsu* and *Fnu* aptamers had near-zero  $-1$  frameshifting whereas the *Tte* aptamer had 3.5% frameshifting at 28°. These results are consistent with SAXS and crystallography data supporting a pre-folded conformation for the apo *Tte* aptamer, and solution and NMR data that show that the apo *Bsu* and *Fnu* aptamers only transiently sample a partially pre-folded state. In addition, the *Fnu* aptamer was the most responsive to preQ<sub>1</sub>, although the level of  $-1$  frameshifting only reached a maximum of 20% even in the presence of 200  $\mu$ M preQ<sub>1</sub>. Replacement of the A–U bps in P1 with G–C bps in the *Fnu* aptamer increased  $-1$  frameshifting to 39% when preQ<sub>1</sub> was present. Yu et al. also found that the EC<sub>50</sub> for this modified *Fnu* aptamer for preQ<sub>1</sub> was 180 nM. Although the K<sub>d</sub> for this construct has not been measured, the most similar construct (*Fnu* WT aptamer) has a reported K<sub>d</sub> of 283 nM [52], indicating that this riboswitch operates under thermodynamic control when regulating translation.

### 5.2. Antibacterial targeting

The prevalence of riboswitches in bacteria makes them attractive targets for antibacterial drug development [77–79]. Riboswitches have already been implemented with some success using ligand mimetics [80–82]. PreQ<sub>1</sub> riboswitches are especially promising as antibiotic targets since preQ<sub>1</sub> is only synthesized in bacteria, preQ<sub>1</sub> riboswitches are therefore only present in bacteria, and Q plays an important role in biology and disease. For example, Q availability is a determinant of virulence for *S. flexneri* [30–33], and the preQ<sub>1</sub>-II riboswitch is found in several virulent *Streptococcal* strains [42]. By developing 7-deazaguanine derivatives to act as preQ<sub>1</sub> mimetics, it may be possible to target these latter virulent bacteria.

### 5.3. Biofuels

Engineering riboswitches for control of protein pathways is being pursued in applications for renewable energy and biofuels due to their ability to perform inducible gene expression. Riboswitches have also been proposed for use in biofuel cells as logic gates [83]. Cyanobacteria are an ideal system for manufacturing biofuels due to their ability to convert light into chemical energy and produce oxygen through oxygenic photosynthesis [84,85]. The synthetic theophylline aptamer has already been used with some success to regulate protein expression in cyanobacteria [86]. PreQ<sub>1</sub>-I is advantageous in biofuel applications due to its small size and ability to regulate at either the transcription or translation level. By taking advantage of the principles governing preQ<sub>1</sub> recognition as well as pseudoknot folding and stability learned from the above studies, the preQ<sub>1</sub> riboswitches can be engineered to attenuate preQ<sub>1</sub> responsiveness in biofuel production.

## 6. Summary

The existence of multiple regulatory mechanisms for Q synthesis indicates its importance in cell fitness. The different structures and dynamics of the preQ<sub>1</sub>-I and preQ<sub>1</sub>-II riboswitches have provided new insights into how RNA can harness control of gene expression using differing modes of recognition of the same ligand. Despite the fact that both classes of preQ<sub>1</sub> riboswitch fold into H-type pseudoknots with preQ<sub>1</sub> at the junction between the two stems, the determinants of ligand specificity, orientation of preQ<sub>1</sub> in the binding pocket, and predicted pathways for ligand capture are very different. The wealth of structural and dynamic information within the two classes, described in this review, has provided insights into how ligand responsiveness can be fine-tuned by altering sequences peripheral to the binding pocket to modulate the binding kinetics and stability of the bound conformation. For example, in the preQ<sub>1</sub>-I riboswitch, variations in the loop 2 sequence and length can modulate preQ<sub>1</sub> binding affinity and pseudoknot stability while the loop 3 sequence may influence kinetics

of ligand recognition. In the preQ<sub>1</sub>-I riboswitch the dynamic loop 2 and unstable P2 help to prevent premature pseudoknot formation and loop 1 (with aid of divalent cations) helps block preQ<sub>1</sub> exit, while in the preQ<sub>1</sub>-II riboswitch the embedded P4 in loop 3 helps to both prevent premature pseudoknot formation and function as a ‘screw’ cap to block ligand exit, although the mechanisms are likely more complex. Although folding and kinetics studies have been reported for the ligand recognition mechanism, no kinetics have yet been measured in the context of transcription or translation control, which will be important for a complete understanding of regulation of gene expression by these riboswitches.

## Acknowledgements

This work was supported by grants from the U.S. Department of Energy (DE-FC03-02ER63421) and the National Institutes of Health (GM48123) to J.F. and a UCLA Tumor Biology USHHS Ruth L. Kirschstein NRSA T32 award (CA009056) to C.D.E.

## References

- [1] J.N. Kim, R.R. Breaker, Purine sensing by riboswitches, *Biol. Cell* 100 (2008) 1–11.
- [2] R.T. Batey, Structure and mechanism of purine-binding riboswitches, *Q. Rev. Biophys.* 45 (2012) 345–381.
- [3] C.G. Edmonds, P.F. Crain, R. Gupta, T. Hashizume, C.H. Hocart, J.A. Kowalak, S.C. Pomerantz, K.O. Stetter, J.A. McCloskey, Posttranscriptional modification of tRNA in thermophilic archaea (Archaeobacteria), *J. Bacteriol.* 173 (1991) 3138–3148.
- [4] F. Harada, S. Nishimura, Possible anticodon sequences of tRNA His, tRNA Asn, and tRNA Asp from *Escherichia coli* B. Universal presence of nucleoside Q in the first position of the anticodons of these transfer ribonucleic acids, *Biochemistry* 11 (1972) 301–308.
- [5] R.C. Morris, M.S. Elliott, Queuosine modification of tRNA: a case for convergent evolution, *Mol. Genet. Metab.* 74 (2001) 147–159.
- [6] D. Iwata-Reuyl, An embarrassment of riches: the enzymology of RNA modification, *Curr. Opin. Chem. Biol.* 12 (2008) 126–133.
- [7] G.A. Garcia, J.D. Kittendorf, Transglycosylation: a mechanism for RNA modification (and editing?), *Bioorg. Chem.* 33 (2005) 229–251.
- [8] H. Grosjean, DNA and RNA Modification Enzymes: Structure, Mechanism, Function, and Evolution, Landes Bioscience, Austin, Tex., 2009.
- [9] J.E. Jackman, J.D. Alfonzo, Transfer RNA modifications: nature's combinatorial chemistry playground, *Wiley interdisciplinary reviews, RNA* 4 (2013) 35–48.
- [10] P.C. Durant, A.C. Bajji, M. Sundaram, R.K. Kumar, D.R. Davis, Structural effects of hypermodified nucleosides in the *Escherichia coli* and human tRNA<sup>Lys</sup> anticodon loop: the effect of nucleosides s2U, mcm5U, mcm5s2U, mmm5s2U, t6A, and ms2t6A, *Biochemistry* 44 (2005) 8078–8089.
- [11] G.R. Bjork, K. Jacobsson, K. Nilsson, M.J. Johansson, A.S. Bystrom, O.P. Persson, A primordial tRNA modification required for the evolution of life? *EMBO J.* 20 (2001) 231–239.
- [12] T.N. Lamichhane, N.H. Blewett, R.J. Maraia, Plasticity and diversity of tRNA anticodon determinants of substrate recognition by eukaryotic A37 isopentenyltransferases, *RNA* 17 (2011) 1846–1857.
- [13] P.F. Agris, F.A. Vendeix, W.D. Graham, tRNA's wobble decoding of the genome: 40 years of modification, *J. Mol. Biol.* 366 (2007) 1–13.
- [14] F. Juhling, M. Mori, R.K. Hartmann, M. Sprinzl, P.F. Stadler, J. Putz, tRNAdb 2009: compilation of tRNA sequences and tRNA genes, *Nucleic Acids Res.* 37 (2009) D159–D162.
- [15] W. Langgut, H. Kersten, The deazaguanine-derivative, queuine, affects cell proliferation, protein phosphorylation and the expression of the proto oncogenes c-fos and c-myc in HeLa cells, *FEBS Lett.* 265 (1990) 33–36.
- [16] W. Langgut, T. Reisser, S. Nishimura, H. Kersten, Modulation of mammalian cell proliferation by a modified tRNA base of bacterial origin, *FEBS Lett.* 336 (1993) 137–142.
- [17] B.T. French, D.E. Patrick, M.R. Grever, R.W. Trewyn, Queuine, a transfer-RNA anticodon wobble base, maintains the proliferative and pluripotent potential of HI-60 cells in the presence of the differentiating agent 6-thioguanine, *Proc. Natl. Acad. Sci. U. S. A.* 88 (1991) 370–374.
- [18] N. Okada, N. Shindo-Okada, S. Sato, Y.H. Itoh, K. Oda, S. Nishimura, Detection of unique tRNA species in tumor tissues by *Escherichia coli* guanine insertion enzyme, *Proc. Natl. Acad. Sci. U. S. A.* 75 (1978) 4247–4251.
- [19] R.K. Owenby, M.P. Stulberg, K.B. Jacobson, Alteration of the Q family of transfer RNAs in adult *Drosophila melanogaster* as a function of age, nutrition, and genotype, *Mech. Ageing Dev.* 11 (1979) 91–103.
- [20] C. Pathak, Y.K. Jaiswal, M. Vinayak, Possible involvement of queuine in regulation of cell proliferation, *BioFactors* 29 (2007) 159–173.
- [21] B.N. White, G.M. Tener, Activity of a transfer RNA modifying enzyme during the development of *Drosophila* and its relationship to the su(s) locus, *J. Mol. Biol.* 74 (1973) 635–651.
- [22] T. Reisser, W. Langgut, H. Kersten, The nutrient factor queuine protects HeLa cells from hypoxic stress and improves metabolic adaptation to oxygen availability, *Eur. J. Biochem./FEBS* 221 (1994) 979–986.
- [23] W. Baranowski, G. Dirheimer, J.A. Jakowicki, G. Keith, Deficiency of queuine, a highly modified purine base, in transfer RNAs from primary and metastatic ovarian malignant tumors in women, *Cancer Res.* 54 (1994) 4468–4471.

- [24] B. Emmerich, E. Zubrod, H. Weber, P.A. Maubach, H. Kersten, W. Kersten, Relationship of queuine-lacking transfer RNA to the grade of malignancy in human leukemias and lymphomas, *Cancer Res.* 45 (1985) 4308–4314.
- [25] B.S. Huang, R.T. Wu, K.Y. Chien, Relationship of the queuine content of transfer ribonucleic acids to histopathological grading and survival in human lung cancer, *Cancer Res.* 52 (1992) 4696–4700.
- [26] S. Ishiwata, J. Katayama, H. Shindo, Y. Ozawa, K. Itoh, M. Mizugaki, Increased expression of queuosine synthesizing enzyme, tRNA-guanine transglycosylase, and queuosine levels in tRNA of leukemic cells, *J. Biochem.* 129 (2001) 13–17.
- [27] S. Ishiwata, Y. Ozawa, J. Katayama, S. Kaneko, H. Shindo, Y. Tomioka, T. Ishiwata, G. Asano, S. Ikegawa, M. Mizugaki, Elevated expression level of 60-kDa subunit of tRNA-guanine transglycosylase in colon cancer, *Cancer Lett.* 212 (2004) 113–119.
- [28] T. Marks, W.R. Farkas, Effects of a diet deficient in tyrosine and queuine on germfree mice, *Biochem. Biophys. Res. Commun.* 230 (1997) 233–237.
- [29] B.A. Carlson, S.Y. Kwon, M. Chamorro, S. Oroszlan, D.L. Hatfield, B.J. Lee, Transfer RNA modification status influences retroviral ribosomal frameshifting, *Virology* 255 (1999) 2–8.
- [30] J.M. Durand, B. Dagberg, B.E. Uhlin, G.R. Bjork, Transfer RNA modification, temperature and DNA superhelicity have a common target in the regulatory network of the virulence of *Shigella flexneri*: the expression of the virF gene, *Mol. Microbiol.* 35 (2000) 924–935.
- [31] J.M. Durand, N. Okada, T. Tobe, M. Watarai, I. Fukuda, T. Suzuki, N. Nakata, K. Komatsu, M. Yoshikawa, C. Sasakawa, vacC, a virulence-associated chromosomal locus of *Shigella flexneri*, is homologous to tgt, a gene encoding tRNA-guanine transglycosylase (Tgt) of *Escherichia coli* K-12, *J. Bacteriol.* 176 (1994) 4627–4634.
- [32] J.K. Hurt, S. Olgen, G.A. Garcia, Site-specific modification of *Shigella flexneri* virF mRNA by tRNA-guanine transglycosylase in vitro, *Nucleic Acids Res.* 35 (2007) 4905–4913.
- [33] B. Stengl, E.A. Meyer, A. Heine, R. Brenk, F. Diederich, G. Klebe, Crystal structures of tRNA-guanine transglycosylase (TGT) in complex with novel and potent inhibitors unravel pronounced induced-fit adaptations and suggest dimer formation upon substrate binding, *J. Mol. Biol.* 370 (2007) 492–511.
- [34] D. Iwata-Reuyl, Biosynthesis of the 7-deazaguanosine hypermodified nucleosides of transfer RNA, *Bioorg. Chem.* 31 (2003) 24–43.
- [35] R.M. McCarty, V. Bandarian, Biosynthesis of pyrrolopyrimidines, *Bioorg. Chem.* 43 (2012) 15–25.
- [36] H. Kasai, K. Nakanishi, R.D. Macfarlane, D.F. Torgerson, Z. Ohashi, J.A. McCloskey, H.J. Gross, S. Nishimura, Letter: the structure of Q<sup>o</sup> nucleoside isolated from rabbit liver transfer ribonucleic acid, *J. Am. Chem. Soc.* 98 (1976) 5044–5046.
- [37] N. Okada, N. Shindo-Okada, S. Nishimura, Isolation of mammalian tRNAAsp and tRNA<sup>Tyr</sup> by lectin-Sepharose affinity column chromatography, *Nucleic Acids Res.* 4 (1977) 415–423.
- [38] J.E. Barrick, K.A. Corbino, W.C. Winkler, A. Nahvi, M. Mandal, J. Collins, M. Lee, A. Roth, N. Sudarsan, I. Jona, J.K. Wickiser, R.R. Breaker, New RNA motifs suggest an expanded scope for riboswitches in bacterial genetic control, *Proc. Natl. Acad. Sci. U. S. A.* 101 (2004) 6421–6426.
- [39] A. Roth, W.C. Winkler, E.E. Reguluski, B.W. Lee, J. Lim, I. Jona, J.E. Barrick, A. Ritwik, J.N. Kim, R. Welz, D. Iwata-Reuyl, R.R. Breaker, A riboswitch selective for the queuosine precursor preQ1 contains an unusually small aptamer domain, *Nat. Struct. Mol. Biol.* 14 (2007) 308–317.
- [40] P.P. Gardner, J. Daub, J.G. Tate, E.P. Nawrocki, D.L. Kolbe, S. Lindgreen, A.C. Wilkinson, R.D. Finn, S. Griffiths-Jones, S.R. Eddy, A. Bateman, Rfam: updates to the RNA families database, *Nucleic Acids Res.* 37 (2009) D136–D140.
- [41] Z. Weinberg, J.E. Barrick, Z. Yao, A. Roth, J.N. Kim, J. Gore, J.X. Wang, E.R. Lee, K.F. Block, N. Sudarsan, S. Neph, M. Tompa, W.L. Ruzzo, R.R. Breaker, Identification of 22 candidate structured RNAs in bacteria using the CMfinder comparative genomics pipeline, *Nucleic Acids Res.* 35 (2007) 4809–4819.
- [42] M.M. Meyer, A. Roth, S.M. Chervin, G.A. Garcia, R.R. Breaker, Confirmation of a second natural preQ1 aptamer class in Streptococcaceae bacteria, *RNA* 14 (2008) 685–695.
- [43] J.A. Liberman, M. Salim, J. Krucinska, J.E. Wedekind, Structure of a class II preQ1 riboswitch reveals ligand recognition by a new fold, *Nat. Chem. Biol.* 9 (2013) 353–355.
- [44] M. Kang, C.D. Eichhorn, J. Feigon, Structural determinants for ligand capture by a class II preQ1 riboswitch, *Proc. Natl. Acad. Sci. U. S. A.* 116 (2014) E663–E671.
- [45] M. Kang, R. Peterson, J. Feigon, Structural Insights into riboswitch control of the biosynthesis of queuosine, a modified nucleotide found in the anticodon of tRNA, *Mol. Cell* 33 (2009) 784–790 (Erratum in: 2010, 2039, 2653–2655).
- [46] D.J. Klein, T.E. Edwards, A.R. Ferre-D'Amare, Cocystal structure of a class I preQ1 riboswitch reveals a pseudoknot recognizing an essential hypermodified nucleobase, *Nat. Struct. Mol. Biol.* 16 (2009) 343–344.
- [47] R.C. Spitale, A.T. Torelli, J. Krucinska, V. Bandarian, J.E. Wedekind, The structural basis for recognition of the PreQ0 metabolite by an unusually small riboswitch aptamer domain, *J. Biol. Chem.* 284 (2009) 11012–11016.
- [48] J.L. Jenkins, J. Krucinska, R.M. McCarty, V. Bandarian, J.E. Wedekind, Comparison of a preQ1 riboswitch aptamer in metabolite-bound and free states with implications for gene regulation, *J. Biol. Chem.* 286 (2011) 24626–24637.
- [49] U. Rieder, K. Lang, C. Kreutz, N. Polacek, R. Micura, Evidence for pseudoknot formation of class I preQ1 riboswitch aptamers, *ChemBiochem* 10 (2009) 1141–1144.
- [50] Q. Zhang, M. Kang, R.D. Peterson, J. Feigon, Comparison of solution and crystal structures of preQ1 riboswitch reveals calcium-induced changes in conformation and dynamics, *J. Am. Chem. Soc.* 133 (2011) 5190–5193.
- [51] D.J. Klein, A.R. Ferre-D'Amare, Crystallization of the glmS ribozyme-riboswitch, *Methods Mol. Biol.* 540 (2009) 129–139.
- [52] U. Rieder, C. Kreutz, R. Micura, Folding of a transcriptionally acting preQ1 riboswitch, *Proc. Natl. Acad. Sci. U. S. A.* 107 (2010) 10804–10809.
- [53] J.K. Wickiser, M.T. Cheah, R.R. Breaker, D.M. Crothers, The kinetics of ligand binding by an adenine-sensing riboswitch, *Biochemistry* 44 (2005) 13404–13414.
- [54] J.K. Wickiser, W.C. Winkler, R.R. Breaker, D.M. Crothers, The speed of RNA transcription and metabolite binding kinetics operate an FMN riboswitch, *Mol. Cell* 18 (2005) 49–60.
- [55] J.A. Liberman, J.E. Wedekind, Riboswitch structure in the ligand-free state, *Wiley interdisciplinary reviews, RNA* 3 (2012) 369–384.
- [56] T. Yamauchi, D. Miyoshi, T. Kubodera, A. Nishimura, S. Nakai, N. Sugimoto, Roles of Mg<sup>2+</sup> in TPP-dependent riboswitch, *FEBS Lett.* 579 (2005) 2583–2588.
- [57] M.J. Cromie, Y. Shi, T. Latifi, E.A. Groisman, An RNA sensor for intracellular Mg(2+), *Cell* 125 (2006) 71–84.
- [58] A. Serganov, A. Polonskaia, A.T. Phan, R.R. Breaker, D.J. Patel, Structural basis for gene regulation by a thiamine pyrophosphate-sensing riboswitch, *Nature* 441 (2006) 1167–1171.
- [59] S. Thore, M. Leibundgut, N. Ban, Structure of the eukaryotic thiamine pyrophosphate riboswitch with its regulatory ligand, *Science* 312 (2006) 1208–1211.
- [60] J. Lipfert, A.Y. Sim, D. Herschlag, S. Doniach, Dissecting electrostatic screening, specific ion binding, and ligand binding in an energetic model for glycine riboswitch folding, *RNA* 16 (2010) 708–719.
- [61] C.E. Dann III, C.A. Wakeman, C.L. Sieling, S.C. Baker, I. Inrov, W.C. Winkler, Structure and mechanism of a metal-sensing regulatory RNA, *Cell* 130 (2007) 878–892.
- [62] K.C. Suddala, A.J. Rinaldi, J. Feng, A.M. Mustoe, C.D. Eichhorn, J.A. Liberman, J.E. Wedekind, H.M. Al-Hashimi, C.L. Brooks III, N.G. Walter, Single transcriptional and translational preQ1 riboswitches adopt similar pre-folded ensembles that follow distinct folding pathways into the same ligand-bound structure, *Nucleic Acids Res.* 41 (2013) 10462–10475.
- [63] P. Banas, P. Sklenovsky, J.E. Wedekind, J. Spomer, M. Otyepka, Molecular mechanism of preQ1 riboswitch action: a molecular dynamics study, *J. Phys. Chem. B* 116 (2012) 12721–12734.
- [64] T. Santner, U. Rieder, C. Kreutz, R. Micura, Pseudoknot preorganization of the preQ1 class I riboswitch, *J. Am. Chem. Soc.* 134 (2012) 11928–11931.
- [65] C.D. Eichhorn, J. Feng, K.C. Suddala, N.G. Walter, C.L. Brooks III, H.M. Al-Hashimi, Unraveling the structural complexity in a single-stranded RNA tail: implications for efficient ligand binding in the prequeuosine riboswitch, *Nucleic Acids Res.* 40 (2012) 1345–1355.
- [66] J. Feng, N.G. Walter, C.L. Brooks III, Cooperative and directional folding of the preQ1 riboswitch aptamer domain, *J. Am. Chem. Soc.* 133 (2011) 4196–4199.
- [67] Z. Gong, Y. Zhao, C. Chen, Y. Xiao, Computational study of unfolding and regulation mechanism of preQ1 riboswitches, *PLoS One* 7 (2012) e45239.
- [68] E.J. Denning, D. Thirumalai, A.D. MacKerell Jr., Protonation of trimethylamine N-oxide (TMAO) is required for stabilization of RNA tertiary structure, *Biophys. Chem.* 184 (2013) 8–16.
- [69] J. Yoon, D. Thirumalai, C. Hyeon, Urea-induced denaturation of preQ1-riboswitch, *J. Am. Chem. Soc.* 135 (2013) 12112–12121.
- [70] K. Han, Y. Byun, PSEUDOVIEWER2: visualization of RNA pseudoknots of any type, *Nucleic Acids Res.* 31 (2003) 3432–3440.
- [71] C.A. Theimer, C.A. Blois, J. Feigon, Structure of the human telomerase RNA pseudoknot reveals conserved tertiary interactions essential for function, *Mol. Cell* 17 (2005) 671–682.
- [72] R.M. Mitton-Fry, S.J. DeGregorio, J. Wang, T.A. Steitz, J.A. Steitz, Poly(A) tail recognition by a viral RNA element through assembly of a triple helix, *Science* 330 (2010) 1244–1247.
- [73] M.F. Souliere, R.B. Altman, V. Schwarz, A. Haller, S.C. Blanchard, R. Micura, Tuning a riboswitch response through structural extension of a pseudoknot, *Proc. Natl. Acad. Sci. U. S. A.* 110 (2013) E3256–E3264.
- [74] J.E. Weigand, B. Suess, Aptamers and riboswitches: perspectives in biotechnology, *Appl. Microbiol. Biotechnol.* 85 (2009) 229–236.
- [75] A. Wittmann, B. Suess, Engineered riboswitches: expanding researchers' toolbox with synthetic RNA regulators, *FEBS Lett.* 586 (2012) 2076–2083.
- [76] C.H. Yu, J. Luo, D. Iwata-Reuyl, R.C. Olsthoorn, Exploiting preQ(1) riboswitches to regulate ribosomal frameshifting, *ACS Chem. Biol.* 8 (2013) 733–740.
- [77] K.F. Blount, R.R. Breaker, Riboswitches as antibacterial drug targets, *Nat. Biotechnol.* 24 (2006) 1558–1564.
- [78] K.E. Deigan, A.R. Ferre-D'Amare, Riboswitches: discovery of drugs that target bacterial gene-regulatory RNAs, *Acc. Chem. Res.* 44 (2011) 1329–1338.
- [79] J. Mulhbach, P. St-Pierre, D.A. Lafontaine, Therapeutic applications of ribozymes and riboswitches, *Curr. Opin. Pharmacol.* 10 (2010) 551–556.
- [80] K.F. Blount, J.X. Wang, J. Lim, N. Sudarsan, R.R. Breaker, Antibacterial lysine analogs that target lysine riboswitches, *Nat. Chem. Biol.* 3 (2007) 44–49.
- [81] J. Mulhbach, E. Brouillette, M. Allard, L.C. Fortier, F. Malouin, D.A. Lafontaine, Novel riboswitch ligand analogs as selective inhibitors of guanine-related metabolic pathways, *PLoS Pathog.* 6 (2010) e1000865.
- [82] C. Ster, M. Allard, S. Boulanger, M. Lamontagne Boulet, J. Mulhbach, D.A. Lafontaine, E. Marsault, P. Lacasse, F. Malouin, Experimental treatment of *Staphylococcus aureus* bovine intramammary infection using a guanine riboswitch ligand analog, *J. Dairy Sci.* 96 (2013) 1000–1008.
- [83] M. Zhou, Y. Du, C. Chen, B. Li, D. Wen, S. Dong, E. Wang, Aptamer-controlled biofuel cells in logic systems and used as self-powered and intelligent logic aptasensors, *J. Am. Chem. Soc.* 132 (2010) 2172–2174.
- [84] L.S. Gronenberg, R.J. Marcheschi, J.C. Liao, Next generation biofuel engineering in prokaryotes, *Curr. Opin. Chem. Biol.* 17 (2013) 462–471.
- [85] B.M. Berla, R. Saha, C.M. Immethun, C.D. Maranas, T.S. Moon, H.B. Pakrasi, Synthetic biology of cyanobacteria: unique challenges and opportunities, *Front. Microbiol.* 4 (2013) 246.
- [86] Y. Nakahira, A. Ogawa, H. Asano, T. Oyama, Y. Tozawa, Theophylline-dependent riboswitch as a novel genetic tool for strict regulation of protein expression in cyanobacterium *Synechococcus elongatus* PCC 7942, *Plant Cell Physiol.* 54 (2013) 1724–1735.
- [87] N.B. Leontis, E. Westhof, Geometric nomenclature and classification of RNA base pairs, *RNA* 7 (2001) 499–512.